Trabajo Fin de Máster
Máster en Ingeniería Química

Study of the effect of CO_2 and steam on char particle temperature and conversion in oxy-fuel combustion in fluidized bed

Autor: Ana Berdugo Vilches

Tutor: Alberto Gómez Barea

Dep. de Ingeniería Química y Ambiental
Escuela Técnica Superior de Ingeniería
Universidad de Sevilla

Sevilla, 2019

Trabajo fin de máster
Máster en Ingeniería Química

Study of the effect of CO2 on char particle temperature and conversion in oxy-fuel combustion in fluidized bed

Autor:

Ana Berdugo Vilches

Tutores:

Dr. Alberto Gómez Barea (Catedrático de Universidad)

Dr. Jesús Salinero Gónzalez

Departamento de Ingeniería Química y Ambiental

Escuela Técnica Superior de Ingeniería

Universidad de Sevilla

Sevilla, 2019

Trabajo Fin de Máster: tudy of the effect of CO2 on char particle temperature and conversion in oxy-fuel combustion in fluidized be

Autor: Ana Berdugo Vilches

Tutor: Dr. Alberto Gómez Barea / Dr. Jesús Salinero Gónzalez

El tribunal nombrado para juzgar el Proyecto arriba indicado, compuesto por los siguientes miembros:

Presidente:

Vocales:

Secretario:

Acuerdan otorgarle la calificación de:

Sevilla, 2019

El Secretario del Tribunal

A mi madre

Acknowledgements

Este trabajo cierra mi última etapa de formación académica y como cualquier otro final de trayecto, ha traído consigo importantes aprendizajes. Durante este camino he tenido la oportunidad de crecer a nivel técnico, pero, sobre todo, a nivel personal, enseñándome la importancia de apoyarse en los demás para caminar hacia tus metas. Puedo decir que he tenido la suerte de encontrar a las personas indicadas en el momento perfecto, que han conseguido aportarme justo lo que necesitaba para conseguir este objetivo. Por ello quiero agradecer a todas las personas que se han cruzado en mi camino durante este recorrido, durante más o menos tiempo, porque gracias a cada uno de ellos he llegado hoy hasta aquí.

En primer lugar, me gustaría mostrar mi mayor agradecimiento a los tres pilares más sólidos e importantes con los que contaré siempre. A mis padres, Rafael y Mª Jesús, por su apoyo constante durante el camino hacia todas las metas que me propongo y a mi hermana, Teresa, por su firme confianza en mi ante cualquier propósito, y porque no existe una ayuda más desinteresada que la que ella me brinda cuando lo necesito.

Por otro lado, quiero agradecer la colaboración de mis compañeros de laboratorio Israel Pardo y Jesús Valera por ayudarme a salvar obstáculos durante el trayecto, y a todos los compañeros que han estado conmigo durante todos estos meses. Asimismo, agradecer a Irene Soriano y a Ellen Augustsson, mis compañeras en Chalmers University of Technology, porque hicieron de mi estancia en Suecia una de las experiencias más enriquecedoras.

De igual modo, me gustaría dar las gracias a David Pallarès y Bo Leckner por su amplio interés en este proyecto y su gran dedicación durante mi estancia en Gotemburgo. Gracias también a Jesús Salinero, quien ha sido mi instructor más cercano, por encontrar siempre la forma de sacar lo mejor de mi.

Por último, quiero mostrar mi más sincero agradecimiento a Alberto Gómez Barea, la persona que ha hecho posible este trabajo, por su confianza, por haberme dado la oportunidad de trabajar en el apasionante mundo de la investigación durante todo este tiempo y por permitirme vivirlo también desde Suecia.

Abstract

In the energy sector, carbon capture has emerged as a technical solution for reducing CO_2 emissions, which are responsible for the greenhouse gas effect and global warming. Oxy-fuel combustion is one of the options for implementing carbon capture. The technology consists of combustion of a fuel with pure oxygen which results in a flue gas stream rich in CO_2 that is suitable for storage. Due to the high temperatures reached inside the boiler, the O_2 is partially dilute with the recycled flue gases, which mainly contents CO_2 (dry recirculation) or CO_2 and water vapor (wet recirculation). Oxy-fuel may be applied in existing power plants which are designed to operate with traditional air combustion (i.e. 1stgeneration). Alternatively, the design of newly built boilers may be improved to enable the operation with higher concentrations of oxygen, thereby reducing the size of the units as compared to the conventional boilers (i.e. 2nd generation). However, the construction of such oxy-fuel combustors requires further knowledge of the fuel conversion process in oxygen-rich environment. Recently a 3rd generation of oxy-fuel combustion has been proposed (i.e. oxy-steam combustion), where the water vapor is directly used as temperature moderator and it avoids the recirculation stream. The literature on oxy-fuel combustion in the presence of steam is still scarce and requires some efforts to clarify its influence on the combustion characteristics. An important aspect is the temperature of the fuel particles, as the high O_2 concentrations in the combustor leads to fast conversion of the fuel, which can result in intolerable temperatures. In this work, the effect of CO_2 and water vapor on the temperature and conversion of the char particles during the combustion process is investigated. A lab-scale fluidized bed reactor is used and the temperature of the char particles is quantified by means of a digital camera. Also, a one-dimensional model is developed to study the influence of H_2O. The results show that the main difference in the temperature and conversion of the fuel particle between oxy-fuel, oxy-steam and air combustion relates to the different diffusivity of O_2 in N_2, CO_2 and H_2O, and the contribution of the gasification reaction under certain conditions.

Resumen

La tecnología de captura de CO_2 es en una de las vías hacia la reducción de las emisiones de CO_2, causantes de la intensificación del efecto invernadero y del calentamiento global. La oxi-combustión es una de las alternativas que permiten implantar esta tecnología. Esta técnica consiste en realizar el proceso de combustión con oxígeno puro, dando lugar a una corriente de gases de combustión rica en CO_2, y que por tanto puede ser capturado de forma viable. Para controlar la temperatura dentro de la caldera, esta corriente de oxígeno puro se diluye parcialmente con ayuda de los gases de combustión, los cuales contienen principalmente CO_2 (recirculación seca) o CO_2 y vapor de agua (recirculación húmeda). La tecnología de oxi-combustión puede instalarse en plantas de producción de energía eléctrica diseñadas para trabajar en combustión con aire (1ª generación), aunque se plantea mejorar esta técnica alimentando mayores concentraciones de oxígeno a la caldera (2ª generación) consiguiendo reducir el tamaño de esta y evitar en un alto grado el caudal de recirculación de gases con respecto a las convencionales. Sin embargo, aún existen una serie de factores que deben ser investigados antes de construir una caldera de 2ª generación. Asimismo, recientemente ha surgido una nueva alternativa (3ª generación) que consiste en utilizar directamente el vapor como moderador de la temperatura, evitando así los costes que supone realizar la recirculación de los gases de combustión. Aún existen pocos trabajos enfocados en estudiar la influencia del vapor en condiciones de oxi-combustión y, por tanto, es necesario profundizar en esta línea antes de implantar una caldera de 3ª generación. Uno de los factores más importantes de estudio es la temperatura de las partículas de combustible, ya que, debido a las altas concentraciones de O_2 en la caldera, la velocidad de conversión de las partículas pude ser muy alta y llegar a un nivel de temperatura inadmisible en el interior de la caldera. En este trabajo se estudia el efecto del CO_2 y el vapor sobre la temperatura y la conversión de partículas de carbonizado de haya. Para las pruebas experimentales se utilizó un reactor de lecho fluido bidimensional (a escala de laboratorio) equipado con una ventana de cuarzo, donde se realizó la combustión de partículas de char. Las medidas de la temperatura superficial de las partículas en combustión se realizan mediante pirometría óptica, utilizando una cámara digital que captura, a través de la ventana, el proceso de conversión. Por otro lado, se ha llevado a cabo un estudio teórico sobre el efecto de la presencia del vapor en oxi-combustión mediante simulaciones en las que, por un lado, el CO_2 se sustituye parcialmente por vapor (recirculación húmeda) y por otro lado, la combustión se realiza en atmósfera de O_2/H_2O. Para ello, se ha desarrollado un modelo numérico, cuyos resultados han sido validados con resultados experimentales obtenidos en las pruebas de combustión del char en atmósfera de O_2/CO_2 y O_2/N_2. Los resultados muestran que las diferencias en la temperatura y conversión de las partículas de char entre los diferentes casos se deben principalmente (i) a la diferencia de difusividad del O_2 en cada uno de los gases utilizados como moderadores de temperatura y (ii) la contribución de la reacción de gasificación del char en determinadas condiciones.

Content

Abstract **xi**

Resumen **i**

Content **i**

Tables **iii**

Figures **iv**

Chapter 1. Introduction **1**
1. Greenhouse effect and global warming *1*
2. CO_2 emissions *2*
3. Oxy- fuel combustion in Fluidized Bed reactor *3*
4. Objectives and contents of this master thesis *6*

Chapter 2. Literature review of the influence of steam in oxy-fuel combustion **9**
1. Steam properties and reactions *9*
2. Effect of partial substitution of CO_2 by H_2O on combustion characteristics *10*
3. Effect of total substitution of CO_2 by H_2O on combustion characteristics *12*
4. Summary and analysis *21*

Chapter 3. Experimental **25**
1. Oxy-fuel combustion experiments *25*
1.1 Preparation of char particles 26
1.2 Experimental set-up 26
1.3 Experimental methodology 27
2. Calibration of the digital camera *28*

Chapter 4. Model development **33**
1. Modes of conversion of a single char particle *33*
2. Modelling approach *34*
3. Model description and formulation *34*
3.2 Transport equations 35
3.3 Boundary conditions: heat and mass fluxes 36
3.4 Discretization and solution 37
1.4 Model parameters 40

Chapter 5. Resuls and discussion **43**
1. The influence of the CO_2 gas concentration on the char temperature and conversion during oxy-fuel combustion in a fluidized bed at high O_2 concentration *43*
2. The predicted effect of steam concentration in oxy-fuel combustion *45*

Chapter 6. Conclusions and further work **49**

Nomenclature **51**

References **53**

Appendix I Analysis methodology **59**

Appendix II Minimum fluidization velocity **61**

Appendix III Inlet gas concentration **63**

Appendix IV Effect of the filter on the radiation captured by the camera **65**
IV.1 Experimental methodology *65*
IV.1 Experimental results *67*

Appendix V. Results and validation of the calibration methodology **69**
1. Experimental results *69*
2. Calculation of the empirical parameter θ_k *69*
2.3 Validation 70

Tables

Table 1.1 Evaluation of candidate system [39] 5

Table 2.1 Comparison of physical properties at 1123ºC and atmospheric pressure [38] 9

Table 2.2 Summary of the steam concentrations studied, and the technology used in each case. FB: Fluidized bed; TGA: Thermogravimetric Analyzer; ER: Entrainer reactor; DTF: Drop tube furnace; HF; Horizontal furnace 21

Table 3.1 Experimental and theoretical studies carried out in this master thesis. 25

Table 3.2 Beech wood properties. 26

Table 3.3 Experimental set up 27

Table 3.4 Operation conditions in the experimental tests. 28

Table 3.5 Calibration experiments 31

Table 4.1. Model parameters 41

Table 4.2 *Kinetic parameters* 41

Table 4.3 Correlations 41

Table AV.0.1 Fitting coefficients for the calibration curves. 70

Figures

Figure 1.1 The difference between the greenhouse effect and enhanced greenhouse effect [3] 2

Figure 1.2. CO_2 emissions in the last few decades and predicted CO_2 emissions assuming different scenarios [6]. 2

Figure 1.3 Primary energy demand by end-use sector, region and fuel [6]. 3

Figure 1.4 Configurations for oxy-fuel combustion systems for dry and wet recycling. ASU: Air separation unit; GRF: Fan for recycled stream; ESP: Electrostatic precipitator [39] 4

Figure 1.5 Schematic diagram of steam-moderated oxy-fuel combustion process. ASU: Air Separation Unit; ESP: Electrostatic precipitator; FGC: Flue gases conditioner; CCS: CO_2 compression, capture and storage unit [33] 6

Figure 2.1 Effect of H_2O concentration on coal combustion behaviour under different O_2 concentrations. (a) Ignition temperature, (b) Burnout temperature [30] 11

Figure 2.2 Prediction results of ignition distance considering (a) the physical properties of steam with oxygen mole fraction of 21%. O_2/CO_2. X, Y, Z, W and b) the chemical properties of steam with oxygen mole fraction of 21%. $O_2/CO_2/H_2O$. X, U, V [27] 11

Figure 2.3 Particles average temperatures, for different coal ranks, during combustion in oxy-fuel atmosphere in regards to H_2O content. [31]. 12

Figure 2.4 Predicted ignition locations change with different pre-exponential factors of the a) WGS reaction and b) gasification reaction in a 30% O_2/70% H_2O atmosphere [35]. 13

Figure 2.5 Ignition delay ratio for different vapor concentrations in mixtures of O_2/H_2O vs O_2/N_2 (a) and $O_2/CO_2/H_2O$ vs O_2/CO_2 (b) with a concentration of O_2 of 21%, calculated from the results of the revised literature. DTF: Drop tube furnace; EFR: Entrained Flow reactor: BC: Bituminous coal; BC-char: Bituminous char 23

Figure 3.1 Beech wood char particle 26

Figure 3.2 Experimental set-up 27

Figure 3.3 Experimental set up in combustion tests 28

Figure 3.4 Capture and interpretation of the radiation from the viewed scene by the digital camera [49].29

Figure 3.5 Experimental set up in calibration tests 30

Figure 3.6 Char particle ready for a calibration test. 30

Figure 4.1 Single char-particle conversion model [56] 34

Figure 4.2 Discretization scene of the model 38

Figure 4.3 Time dependent external boundary conditions scene: a) initial particle size, b) particle size when the local conversion (x_c) of the three outer nodes have reached 98%. r_{ext} is the external particle radius. 40

Figure 5.1 Effect of the fluidization flow, O_2/N_2 (filled symbol) vs. O_2/CO_2 (empty symbol), on the apparent consumption rate: r_c by Eq. 1 (a) and on the maximum temperature: $T_{c,max}$ (b) of char particles from 43

Figure 5.2 Measured surface temperature of a char particle from beech wood (8mm) in a fluidized bed at 800 ºC with an O2 concentration of 40 and 60 %v/v in N2 (empty symbols) and in CO2 (filled symbols). Star symbol: particle temperature in the emulsion phase. Square symbol: particle temperature in the splash zone and the bubble phase. 44

Figure 5.3 Predicted (solid line) and measured (symbol) evolution of a surface beech wood particle temperature (8 mm) during its conversion, in a fluidized bed at 800 ºC with an O_2 concentration of 60 %v/v in N_2 (empty symbols) and in CO_2 (filled symbols) 45

Figure 5.4 Experimental and predicted burnout time of a char particle from beech wood in a fluidized bed at 800 ºC with an O_2 concentration of 21, 40, 50, 60 and 70 %v/v in a) CO_2 with (solid line) and without (dotted line) gasification reaction considered in the simulation and b) N_2. Filled symbol: experimental burnout time. 45

Figure 5.5. Predicted burnout time and maximum temperature of a char particle from beech wood in a fluidized bed at 800 ºC with an O_2 concentration from 10 to 60 %v/v in N_2 (green) CO_2 (red) and H_2O (blue). Symbol: experimental data. Solid line: Predicted data 46

Figure 5.6 Concentration profile of O_2 in a) oxy-CO_2 and b) oxy-steam process for a beech wood char particle at 200 second of reaction. 46

Figure AI.0.1 Maximum and minimum temperature of biomass char particle surface for the combustion tests carried out at 60% O_2 concentration in N_2. 59

Figure AI.0.2 Last image found in a combustion test. 60

Figure AI.0.1 Pressure drop in the distributor (a) and addition of the pressure drop in the distributor plus in the material bed 61

Figure AII.0.2 Pressure drop curves using air, N2 and CO2 as inlet gas flow. 62

Figure AIII.0.1 O_2 concentration calculated vs measured at the reactor inlet in O_2/N_2 (a) and O_2/CO_2 (b) atmosphere. 63

Figure AIV. 0.1 Results of maximum temperatures obtained in previous works using biomass char particles in combustion tests in O2/N2 atmosphere at different O2 concentration, from 11% to 40% [26] . 65

Figure AIV. 0.2 Experimental set up for the experiments to understand the effect of the filter. 66

Figure AIV.0.3 Selected area used on the temperature analysis 66

Figure AIV.0.4 Digital numbers red (I), green (II) and blue (III) assigned by the camera when the filter is not used (A) and when the filter has the position 1 (B), 2 (C) and 3 (D), versus the temperature measured with thermocouple. 67

Figure AIV.0.5 DN-T curves for each spectral band (red(I), green(II) and blue(III)) in case A (without filter), case D (filter in the last position) and DNk-T curves calculated using the direct proportional relation between case A and D (eq. AIV.1). 68

Figure AV0.2 Precision of the pyrometry method in the three spectral bands. (a) Range of temperatures measured by the thermocouple for each temperature indicated by the pyrometry method. (b) Absolute error according to (3.4) Each band is represented in its own color. $T_{thermocouple}$: temperature shown by the thermocouple. $T_{pyrometric}$: temperature measured by the pyrometry method. 71

Figure 0.3 Minimum and maximum particle temperature measured by pyrometry over conversion time of a beech particle of 8mm diameter (a) 21% O_2/N_2; (b) 40% O_2/N_2. Blue symbols from Salinero et al. [26]. Black symbols from this work. 72

Figure 0.4 Maximum superficial temperature of the char particle versus O_2 in N_2. Filled symbols: results with filter from this work. Empty symbols: results without filter from Salinero et al. [26]. 72

Chapter 1. Introduction

This chapter shows a brief description about the current energy situation and explains the need to reduce the CO_2 emissions. Among all proposed technologies, oxy-fuel combustion in a fluidized bed is one of the most promising routes. The main efforts for the development of this technology have been focuse toward clarifying the influence of changing the gas environment from O_2/N_2 to O_2/CO_2 on the temperature and conversion of a fuel particle. Most research has been focused on studying this effect, however, the water content in the recycled stream could also influence the characteristics of the combustion. Likewise, oxy-fuel combustion using steam as a temperature moderator has recently emerged as the third generation of this technology. Therefore, the presence of steam in oxy-fuel combustion is studied in the present work.

1. Greenhouse effect and global warming

The greenhouse effect is a natural process that warms the Earth's surface. When the Sun's energy reaches the Earth's atmosphere, some of it is reflected back to space and the rest is absorbed and re-radiated by greenhouse gases (Figure 1).

Greenhouse gases include water vapor, carbon dioxide, methane, nitrous oxide, ozone and some artificial chemicals such as chlorofluorocarbons (CFCs). The absorbed energy warms the atmosphere and the surface of the Earth. This process maintains the Earth's temperature at around 33 degrees Celsius warmer than it would otherwise be, allowing life on Earth to exist. [1].

The strength of the greenhouse effect (how much extra energy it directs toward the earth's surface) depends on how many greenhouse gas molecules there are in the atmosphere. When greenhouse gas concentrations are high, they absorb a greater percentage of the earth's infrared energy emissions. This means that more energy gets reemitted back toward the earth's surface, raising its average surface temperature [2] (Figure 1.1).

Human activities, particularly burning fossil fuels (coal, oil and natural gas) are increasing the concentrations of greenhouse gases [4]. This is the enhanced greenhouse effect, which is contributing to warming of the Earth.

Carbon dioxide (CO_2) accounts for around three-quarters of the warming impact of current human greenhouse-gas emissions [5].

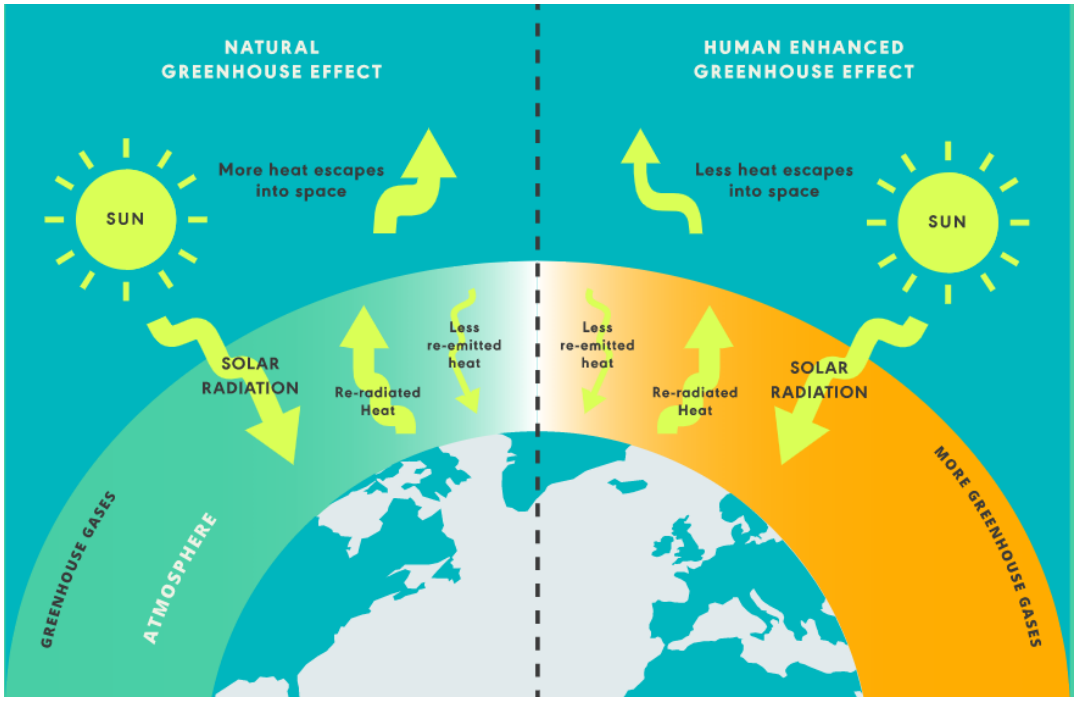

Figure 1.1 The difference between the greenhouse effect and enhanced greenhouse effect [3]

2. CO_2 emissions

CO_2 emissions have become an increasing concern over the last few decades. According to the "Energy Outlook 2019", considering an "evolving transition" scenario, which assumes government policies, technologies and societal preferences evolve in a manner and speed similar to the recent past, these emissions will be increased to around 40% in 2040 (Figure 1.2.) caused by an increase in energy demand [6].

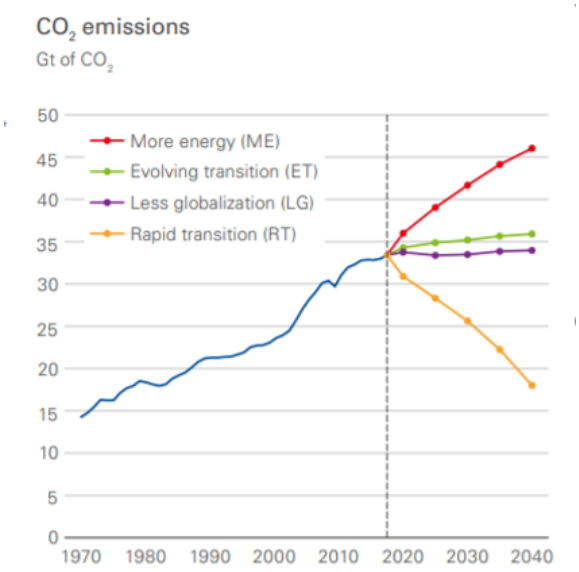

Figure 1.2. CO_2 emissions in the last few decades and predicted CO_2 emissions assuming different scenarios [6].

British oil company BP estimates that global energy demand will be a third higher in 2040 due to the rapid growth of developing economies, mainly those in India, China and other regions of Asia (Figure 1.3b), and, according to Figure 1.3a, the energy consumed by industry and the construction sector accounts for 75% of that increase.

Likewise, Figure 3c, represents the global energy mix in the next years. The most diverse energy mix the world has ever seen is presented in 2040 [6], with oil, gas, coal and non-fossil fuels each contributing around 25%.

This fact means that carbon burning will continue to be an important source of energy. Therefore, there is a need of reduction of CO_2 emission, which involves both increase in the efficiency of power plants and CO_2 capture and storage (CCS).

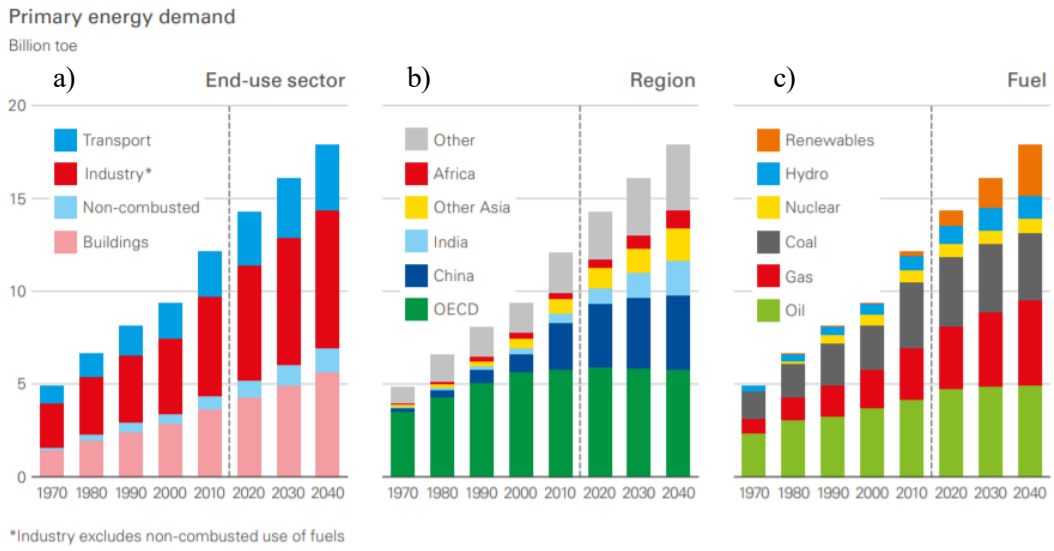

Figure 1.3 Primary energy demand by end-use sector, region and fuel [6].

3. Oxy- fuel combustion in Fluidized Bed reactor

Oxyfuel combustion is one of the leading technologies considered for capturing CO_2 from power plants with CCS. It involves the process of burning the fuel with nearly pure oxygen instead of air.

To capture the CO_2 from a power plant, the main purpose of using this technology is to generate a flue gas with high concentration of CO_2 and water vapor; and then separate the CO_2 from the flue gas by dehydration and low temperature purification processes. Furthermore, this technology reduces NOx and SO_2 emissions compared to conventional combustion technology [7] where, on the one hand, NOx reduction occurs as a result of the low concentration of N_2 in the boiler and the interaction of the NOx recirculated with the hydrocarbons generated (reburning) [8] and, on the other hand, the lower amount of SO_2 in the gases is due to the greater sulfur retention by ashes sulphation [9,10].

Combustion under these conditions may produce high temperature during the conversion process. In order to control the flame temperature, some part of the flue gas is recycled back into the furnace/boiler. The recycled stream is constituted, mainly, by CO_2 (dry recycling). Combustion process under O_2 / CO_2 atmosphere presents several differences from O_2 / N_2 atmosphere. Many of the effects can be explained by the differences in the properties of both gases such as density, heat capacity, diffusivity or radiant properties [11].

The first generation of oxy-boilers involves the retrofitting of the combustion power plants where the flue gas recirculation keeps almost similar condition inside the boiler as the ones in an air-combustion boiler: an O_2 concentration between 25% and 35%v/v [12]. Although the first generation reduce the CO_2 emissions, oxy-

boilers can be conceived with higher O_2 concentration leading to a second generation of oxy-boilers. Such second generation would increase the plant efficiency and reduce the volume of the gases through the boiler.

Since pulverized coal is the main type of fuel in existing power plants, most of the research is focused on these pulverized fuel boilers [13-18]. However, FB reactors could be a more suitable technology because the bed particles moderate the conversion temperatures (by its large thermal capacity) while transferring the heat to the receiving surfaces of the boiler, reducing the flue-gas recirculation and the reactor size [19,20]. Moreover, they can be operated with low-grade fuels, having low heating value and high ash content, including not only coals but also biomasses and/or wastes.

Regarding the oxyfuel combustion conditions, most research in fluidized beds have been conducted with dry recirculation (CO_2) and in O_2 concentration up to 40%[21-25]. In previous works the authors tried to measure in an atmosphere up to 50% O_2 [26]. Additionally, latest trends in oxy-fuel combustion have focused on wet recirculation (CO_2 and H_2O) [27-32] and even more recently on using steam as a temperature moderator [33-37]. The water content in the recirculation stream could have an impact on the characteristics of the combustion and on the efficiency of the plant [38]. Nakayama et al. [39] proposed five configurations for dry and wet oxy-fuel combustion systems (Figure 4) in order to evaluate their efficiency and economic viability. The configurations are different in the position of the recycled stream and the O_2 preheater. Changing the position of these units will have an impact on the size of both the preheater, the electrostatic precipitator (ESP), and the flue gas cooling unit (Table 1.1).

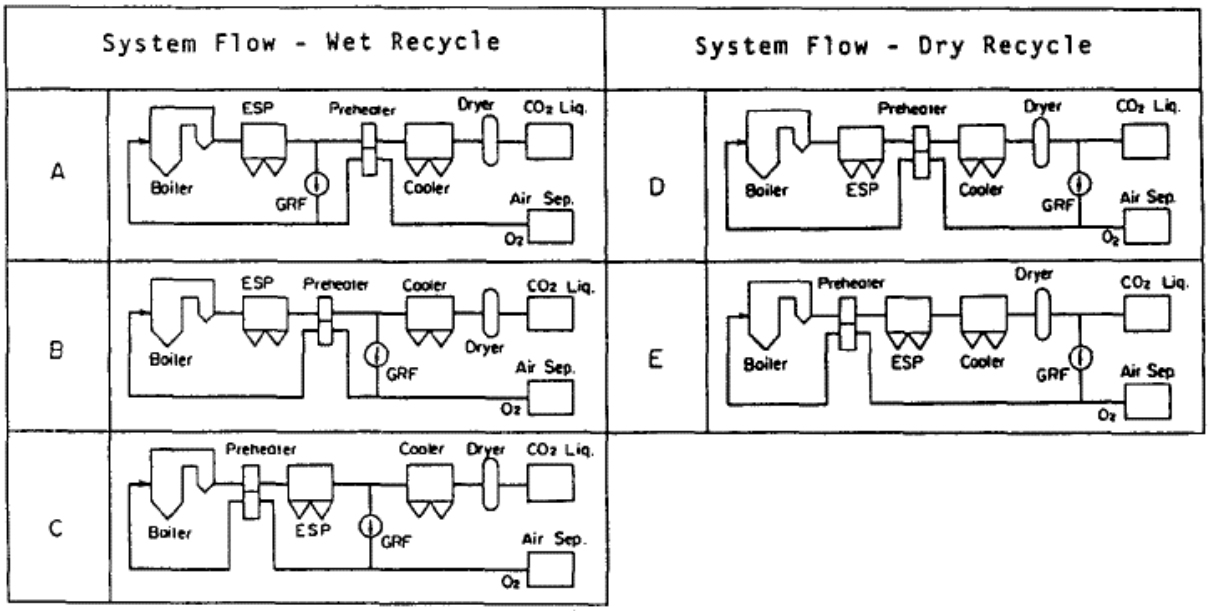

Figure 1.4 Configurations for oxy-fuel combustion systems for dry and wet recycling. ASU: Air separation unit; GRF: Fan for recycled stream; ESP: Electrostatic precipitator [39]

Table 1.4 shows comparison of the feasibilities of conceivable system configurations. Based on this comparative assessment the authors found that dry recycle process is disadvantageous in terms of initial and operating costs because its gas cooler (oxygen preheater) and dryer are required to have a very large capacity [39].The authors concluded that a wet recycle process, particularly the configuration which recycles flue gas after cooling it (system B), was the most promising configuration, according to the assessment. The evaluation was based on theoretical considerations and no experiments were carried out to test the effect of wet and dry recycle on the combustion process.

Table 1.1 Evaluation of candidate system [39]

	O_2 Preheater	ESP	Gas Cooling & Drying	Gas Recircu-lation Fan	Total Evaluation
A	◎	○	○	△	△
B	○	○	○	○	○
C	×	◎	○	○	×
D	○	○	△	◎	△
E	×	◎	△	◎	×

INDICATER:
◎ :very good, ○ :good, △ :not so good, × :bad

On the other hand, studies carried out in an installation (~ 3 kWt) of bubbling fluidized bed, using coal as fuel, showed that the oxy-fuel combustion with wet recycle configuration was beneficial in comparison with the dry recycling for the purposes of NO emissions [40,41]. Using this one, they concluded that the NO concentration decreased with the presence of water vapor in the recycled stream.

Oxy-fuel combustion using steam as a temperature moderator come to be the third alternative technology. In 2007, Salvador et al. proposed a new method of oxy-fuel, called "oxy-steam combustion" [42]. In this new system, the conversion of the fuel into pure oxygen takes place, and steam or water is used as the moderator of the high temperature. Experiments in pilot plant (0.2 MWth) and simulations (CFD) showed that, using the new configuration, the levels of CO and NOx decreased compared to the conventional system and the CO_2 concentration was about 90% [42].

Seepana et al. [43] proposed a system based on oxy-fuel combustion with steam called "steam-moderated oxy-fuel combustion" (SMOC). The Figure 1.5 shows a scheme of the proposed system [33]. Using this configuration, there is no combustion gas recycled stream. Oxygen of purity from the air separation unit is mixed with the steam. This oxidant is then fed to the boiler to combust the fuel.

At the boiler exit, the flue gas consists primarily of steam and to a lesser extent CO_2, excess O_2, N_2, etc. The flue gas is sent first to an ESP for ash particulate removal then to the secondary energy recovery system to produce the steam required for temperature moderation, and finally to a flue gas conditioner (FGC) in which most of the steam is condensed. By putting the ESP after the secondary energy recovery systems, the operating temperature of the ESP can be reduced leading to further reduction in size, however, in the case described by Seepana et al. [43] the ESP is located upstream of the heat exchanges in order to reduce the erosion damage of the internals, which is an important consideration for high ash coals.

The water from the FGC is recycled to generate steam for boiler injection, the dry combustion gas is sent to a CO_2 compression, sequestration and storage system.

Related to the amount of steam required in the boiler, L. Sheng et al.[55] found, during its simulation of an oxy-steam system by Aspen Plus, that at the start-up, the oxy-steam combustion boiler is at the dynamic change, and the water purely generated from the coal combustion was much less than the required amount, so the extra sources, like steam turbine was required to supply the make-up steam. However, when the system came into the steady state, the condensed water generated from flue gas condensation in FGC is more than was enough to supply the required steam. Heating the recycled condensed water generated the enough steam required.

The advantages of the proposed steam-moderated oxy-fuel combustion over conventional flue gas recycling for oxy-coal combustion are as follows [33]:

i) The overall system is simple (no combustion gas recycled stream).

ii) The pumping costs associated with recycling are relatively low because the transmission medium is liquid water but not flue gas.

iii) The formation of NOx and SOx in the boiler can be reduced owing to the use of steam as combustion moderator.

iv) The specific heat of the steam is lower than that of the CO_2 (Table 2.1), so less amount of steam is needed to achieve the same combustion temperature in oxy-steam combustion as compared to O_2/CO_2 recycled combustion. The sizes of the major and auxiliary equipment of the system are smaller than those of the O_2/CO_2 recycled combustion system.

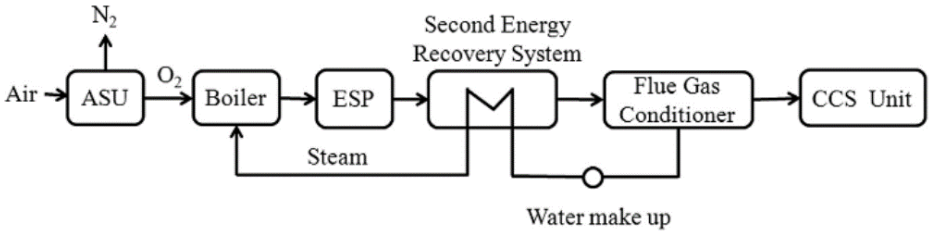

Figure 1.5 Schematic diagram of steam-moderated oxy-fuel combustion process. ASU: Air Separation Unit; ESP: Electrostatic precipitator; FGC: Flue gases conditioner; CCS: CO_2 compression, capture and storage unit [33]

However, the primary disadvantages of oxyfuel combustion (both oxy-CO_2 and oxy-steam combustion cases) are the very high energy requirement for producing high purity O_2.

The literature on oxy-fuel combustion in the presence of steam is still scarce and a detailed review of the most relevant works is presented Chapter 2.

The choice of a measurement technique for the temperature of a fuel particle in a fluidized bed is difficult, as the technique must allow the free movement of the fuel particle as well as to be able to detect the particle in the different phases and zones of the fluidized bed. Thermocouples [22-25, 45] have been, by far, the most applied technique despite its limitations. It has been shown recently that this measurement technique impacts the fuel particle conversion in an FB [46, 47]. Few authors have tried alternative techniques such as electromagnetic-based probes [48], alloy rings [44] and pyrometry [26]. So far, pyrometric techniques seem the most promising technique as it is not intrusive, thereby not interfering with the particle properties and free movement. Therefore, pyrometry has been chosen in this work as a measurement technique for the temperature.

4. Objectives and contents of this master thesis

The aim of the present work is studying the conversion of a single char particle in fluidized bed under oxy-fuel combustion conditions that are relevant to the current trends in the field, i.e. O_2 concentrations above 35% and in the presence of water vapor. This thesis encompasses both experimental and theoretical modeling work, where the model is conceived to cover oxy-combustion conditions at high O_2 concentrations. The effect of high O_2 concentration on the combustion characteristics (i.e. fuel particle temperature and conversion) of the fuel particle is explored experimentally (by pyrometry) and described with the model. The influence of water vapor is explored theoretically and compared to the use a CO_2 flow (dry recirculation) as a temperature moderator.

The objectives and main tasks of this study are:

I) Description of the influence of O_2 concentrations above 35% on oxy-fuel combustion, and the reactions involved.

- Calibration of the digital camera to carry out the experimental measurements.
- Planning and execution the experimental tests. Build a kinetic model of a single char particle.
- Validate the model using the experiments performed with different oxygen concentrations.

II) Description of the influence of the steam properties, as well as the reactions involved, on the fuel particles combustion.

- Analysis of some of the most relevant works about the effect of steam in oxy-fuel combustion, in order to synthetize the existing information, identifying the main gapsin the field needing further reasearch.
- Include the physicochemical effects of steam in the model above, taking into account both char combustion (with O_2) and gasification (with CO_2/steam).
- Compare the theoretical results of the oxy-fuel combustion in presence of steam ("oxy-steam"and oxy-fuel combustion with wet recycled) with those obtained for traditional combustion (O_2/N_2 atmosphere) and oxy-fuel combustion with dry recirculation (O_2/CO_2 atmosphere).

Chapter 2.
Literature review of the influence of steam in oxy-fuel combustion

Some relevant works about oxy-fuel combustion in presence of steam are reviewed in order to analyze the effect of steam in the experiments performed by some authors.

1. Steam properties and reactions

Due to the differences between the physicochemical properties of H_2O, N_2 and CO_2 (Table 2.1), the combustion characteristics in presence of steam are different from those in conventional air combustion and oxy-CO_2 combustion.

Table 2.1 Comparison of physical properties at 1123ºC and atmospheric pressure [38]

	H_2O	O_2	N_2	CO_2
Density (ρ) [kg/m^3]	0.157	0.278	0.244	0.383
Thermal conductivity (k) [W/m K]	0.136	0.087	0.082	0.097
Specific heat capacity (c_p) [kJ/kmol K]	45.67	36.08	34.18	57.83
Specific heat capacity (c_p) [kJ/kg K]	2.53	1.00	1.22	1.31
Heat sink (ρc_p) [kJ/m^3 K]	0.397	0.278	0.298	0.502
Dynamic viscosity (μ) [kg/m s]	5.02e-05	5.81e-05	4.88e-05	5.02e-05
Kinematic viscosity (ν) [m^2/s]	3.20e-04	2.09e-04	2.00e-04	1.31e-04
Mass diffusivity of O_2 in X ($D_{O_2/X}$) [m^2/s]	–	–	1.7e-04	1.3e-04

Additionally, when steam participates in the combustion atmosphere, the following reactions take place:

$$C + H_2O \rightarrow CO + H_2 \qquad \Delta H_{298\,K} = +130\ kJ/mol \tag{1}$$

$$CO + H_2O \rightarrow CO_2 + H_2 \qquad \Delta H_{298\,K} = -40\ kJ/mol \tag{2}$$

$$H_2 + \frac{1}{2}O_2 \rightarrow H_2O \qquad \Delta H_{298\,K} = -242\ kJ/mol \tag{3}$$

Where (1) represents the gasification reaction of carbon with steam, (2) is the water gas shift (WGS) reaction and (3) the combustion of H_2.

The studies reviewed have worked with steam concentrations from 5% to 80%, in different gas mixtures of $O_2/CO_2/H_2O$ (partial substitution of CO_2 by H_2O) and O_2/ H_2O (total substitution of CO_2 by H_2O).

2. Effect of partial substitution of CO_2 by H_2O on combustion characteristics

Riaza et al. [28] measured the ignition temperature and combustion rate of pulverized coal, using different O_2/N_2 and O_2/CO_2 concentrations, in absence and presence of water vapor in an entrained flow reactor. The operating conditions of these tests and that of some authors are presented in Table (Table 2.5). The results show that when steam was present in the combustion process: (i) the coal particle ignited at higher temperature (higher ignition delay) and (ii) lower coal burnout value were observed (lower conversion rate), (iii) no significant differences were found between the different steam concentrations (5%, 10%, 20%). The lower coal burnout value and higher ignition delay in presence of steam, compared with the air-combustion case, could be explained by the higher molar specific heat of H_2O (v) compared to N_2. However, they found no increase in burnout when steam was added that under oxy-fuel atmospheres, although the molar specific heat of water vapor is lower than that of CO_2. Therefore, they concluded that other factors must influence oxy-fuel combustion with the addition of steam such as radiation (i.e enhancements in thermal radiation due to the higher gas emissivity in the oxy-wet compared with the oxy-dry case [11]) and endothermal radical formation (O, OH, H, etc.).

Gil et al. [29] also found no relevant differences between the different steam concentration during a thermogravimetric analysis of different types of pulverized coal (Table 2.5). The authors found opposed results related with the ignition process and burnout in presence of steam.

The parameters studied by Gil et al. [29], and the rest of authors reviewed below that applied the TGA as experimental method [30, 36, 33], are ignition temperature, burnout temperature and peak temperature. Such parameters are defined as follow:

i) Ignition temperature (T_i), defined as the temperature at which a mass loss increases from 1%/min.
ii) Burnout time (T_h), defined as the temperature at which the rate of mass loss decreases from 1%/min.
iii) Peak temperature (T_{max}), defined as the temperature at which the greatest loss of mass occurs.

The authors [29] found that the replacement of CO_2 with 10-20% of steam shifted the DTG curves to lower temperatures (T_i, T_h and T_{max} are lower in presence of H_2O) and generally caused a decrease in combustion time with respect to those in the 21%O_2/79%CO_2 or 30%O_2/70%CO_2 oxyfuel combustion atmospheres. According to these authors, explanation of their results is based on the lower molar specific heat of steam in relation with CO_2. This fact leads to an increase in particle temperature and therefore, to an increase in the conversion rate.

Similar studies, using thermogravimetric analyses, at higher H_2O concentrations (up to 40%) were conducted by Yi et al. [30]. The authors study the influence of the H_2O concentration on coal in $O_2/CO_2/H_2O$ atmosphere at different O_2 concentrations (i.e. 21%, 30% and 40%). They found that the impact of H_2O on burnout temperature varies with the O_2 concentration. The results are shown in Figure 2.1.

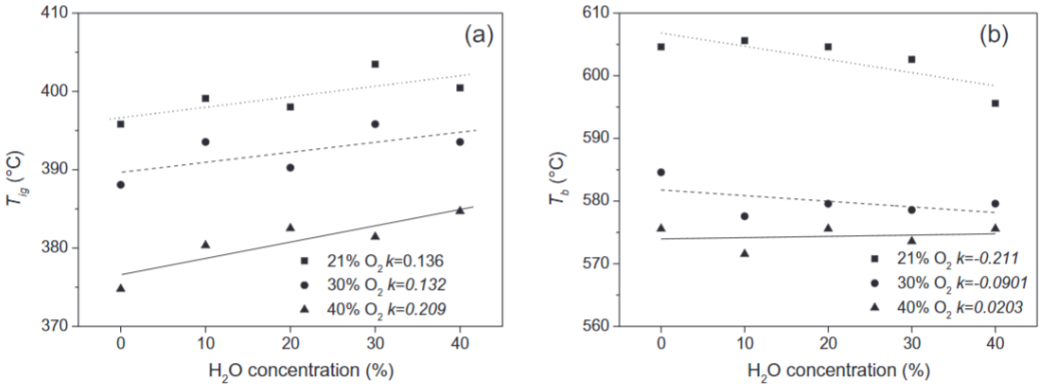

Figure 2.1 Effect of H_2O concentration on coal combustion behaviour under different O_2 concentrations. (a) Ignition temperature, (b) Burnout temperature [30]

It seems that as the oxygen concentration increases, the decreasing tendency of burnout temperature gradually slows, and is essentially constant at 40% O_2. However, at the same time, there was an increase in the ignition temperature (i.e. the opposed result than Gil et al. [29]).

Cai L. et al. [27] studied the effect of steam on the ignition distance, of pulverized coal particles, in different oxy-fuel atmospheres (i) by performing several experiments in a drop tube furnace and (ii) by a "CFD" simulation. They found experimentally that, when the O_2 concentration was greater than 40% the behavior of the ignition process in the presence of steam (5% and 20%) was like the case in which the steam was absent. However, when O_2 concentration was 30%, the ignition process come earlier than the previous cases. This result shows that the effect of the steam decreases with the molar fraction of O_2 (the same behavior as that found by Gil et al. [29]).

They attribute this effect to the different physical and chemical properties of steam compared with CO_2 and, in order to evaluate the contribution of each physico-chemical properties to the ignition process they carried out a sensitivity analysis by using identical mixtures of $O_2/CO_2/H_2O$, $O_2/CO_2/X$ (or Y, Z, W…). This third unknown component of the mixture (X, Y, Z…) was an artificial material that was introduced to substitute steam in the simulations and it had been designed by selecting the physico-chemical properties values desired to study the influence of each one in the ignition location (Figure 2.2).

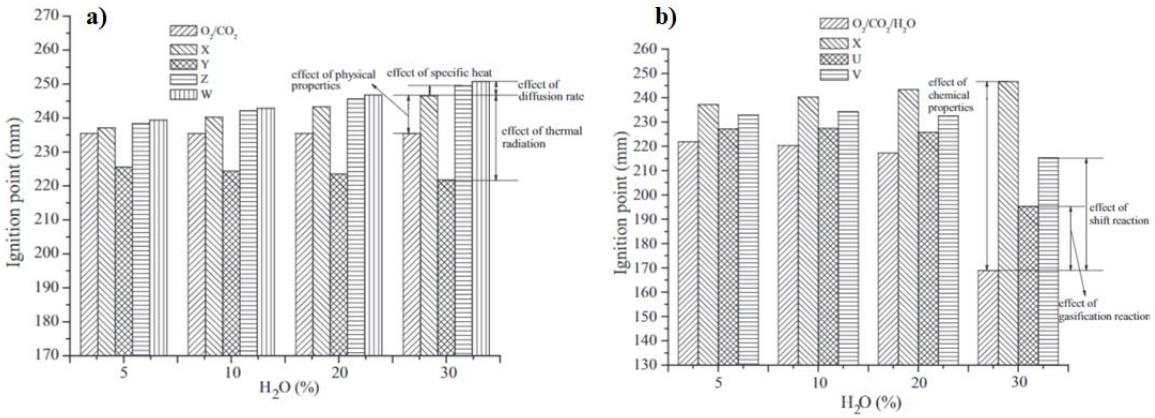

Figure 2.2 Prediction results of ignition distance considering (a) the physical properties of steam with oxygen mole fraction of 21%. O_2/CO_2. X, Y, Z, W and b) the chemical properties of steam with oxygen mole fraction of 21%. $O_2/CO_2/H_2O$. X, U, V [27]

From their study, they conclude that the WGS reaction is the primary reason, and the steam gasification is a minor reason for the advanced ignition of coal particles in O_2/H_2O atmospheres for the presence of high mole fractions of steam.

Related to the study of combustion in millimeter coal particles, Marek et al. [31], recorded the char particles temperature during its combustion in a horizontal furnace under different oxy-fuel combustion atmospheres, and measured the particle temperature combustion by a thermocouple. Their results show that the addition of vapor in oxy-fuel combustion (i.e. $O_2/CO_2/H_2O$) increased the particle temperature during its conversion compared with the oxy-CO_2 case (Figure 2.3).

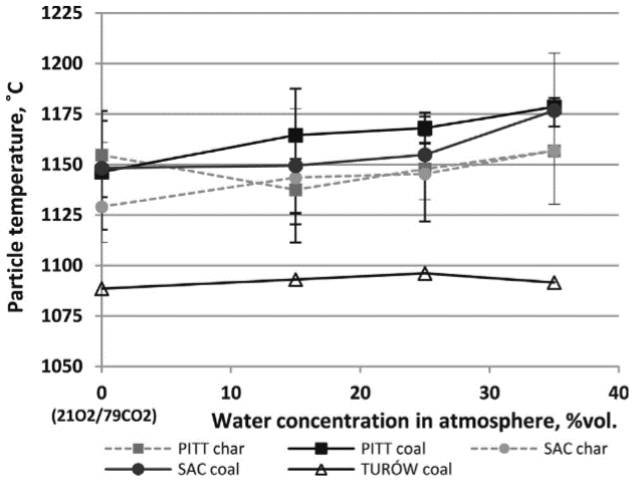

Figure 2.3 Particles average temperatures, for different coal ranks, during combustion in oxy-fuel atmosphere in regards to H_2O content. [31].

Similar results were obtained by Roy et al [32] by doing experiments in a fluidized bed reactor (operating conditions are shown in Table Figure 2.5). These authors observed around 30°C peak temperature difference between char in the dry oxy-fuel combustion environment with 10% oxygen concentration, while around 48°C using 15% steam in the oxy-fuel combustion atmosphere with same 10% oxygen concentration.

The authors attributed this effect both to H_2O lower than CO_2 specific molar heat and more promoted, less energy demanding H_2O gasification reaction ($\Delta H_{C+H2O} = 130 \frac{kJ}{mol}$ vs $\Delta H_{C+CO2} = 167 \frac{kJ}{mol}$).

3. Effect of total substitution of CO_2 by H_2O on combustion characteristics

Zou C.et al. [33] carried out a thermogravimetric analysis in order to study the effect of changing from O_2/N_2 to O_2/H_2O with equal volumetric fractions of O_2 (21%,30%, 40% and 80%), on the ignition delay and burnout time.

The results showed that in both cases (i.e. traditional combustion and oxy-steam combustion) the (i) higher the O_2 concentration the higher the combustion rate (ii) T_i and T_h increased by increasing the particle size (due to larger specific surface area of fine particles), (iii) The characteristic temperatures were higher for the highest-ranking coal, (iv) the ignite temperature, T_i, and burnout temperature, T_h, in oxy-steam combustion is higher than those in O_2/N_2 mixtures combustion with equal oxygen concentration (due to the thermo-physical difference of combustion atmospheres) and

(v) the differences of the characteristic temperatures between O_2/H_2O atmosphere and O_2/N_2 atmosphere decrease as oxygen concentration is increased (less influence of physical properties differences between steam and N_2 on coal combustion characteristics).

However, the same authors [34] carried out more experiments in a tubular furnace by using monitoring techniques (see Table 2.6 for operating conditions) and different results were shown. During this study the behavior of the ignition process was recorded using a high-speed camera, and the particle temperature was measured during ignition by a pyrometer. According to the captured images, (i) the coal ignition in H_2O atmosphere took place earlier than in O_2/N_2 at identical O_2 concentrations, (ii) an increase in the concentration of O_2 caused an increase in image intensity and (iii) the combustion of the volatiles around the particle was completed earlier in H_2O than in N_2. In addition, the particle temperature measurement indicated, on the one hand, an increase in temperature with the fraction of O_2, in both atmospheres (i.e. O_2/N_2 vs O_2/H_2O) and, on the other hand, a higher temperature for the oxy-fuel combustion case with steam for similar O_2 concentrations in N_2.

These results were validated by CFD model developed by Cai L et al. [35]. By means of a "CFD" model these results were studied and validated by Cai L et al. [35]. According to these authors, the effects of steam on coal ignition are due to the physical and chemical properties of steam,(i.e., higher mole specific heat than N_2 is beneficial in the delay of ignition, and steam gasification reaction and WGS reaction may be associated with the advanced ignition in O_2/H_2O atmospheres compared with that in O_2/N_2 atmospheres [35]). To evaluate the contribution of these effects Cai et al. [35] adopted a sensitivity analysis for the combustion mechanism using the "CFD" simulation. They changed the pre-exponential factor for WGS reaction (Figure 2.4 a) and for steam gasification reaction (Figure 2.4 b) and studied the effect on the theoretical ignition location, concluding that the WGS reaction was the main reason for the early ignition in H_2O compared with O_2/N_2 atmosphere.

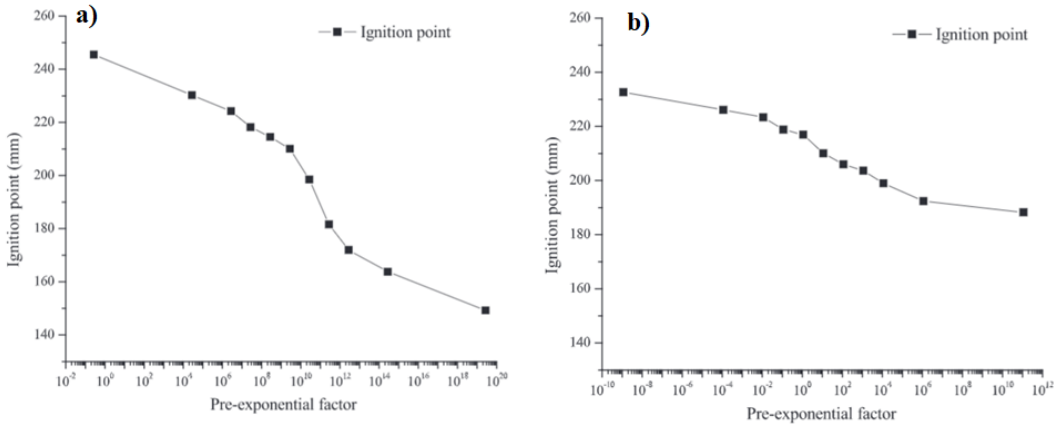

Figure 2.4 Predicted ignition locations change with different pre-exponential factors of the a) WGS reaction and b) gasification reaction in a 30% O_2/70% H_2O atmosphere [35].

Liang et al. [36] drove similar conclusions by measuring the characteristic combustion temperatures of two types of char. Their study consisted of measuring the characteristic combustion temperatures defined for two types of char. Lower values for T_i, T_h and T_{max} for combustion in H_2O atmosphere case were found compared to N_2. They concluded that reaction_under oxy- fuel combustion conditions in presence of steam was faster than for conventional oxy-fuel combustion. They attributed this effect to the fact that O_2 has a diffusivity coefficient in H_2O greater than in N_2.

All of these authors focused on comparing the characteristics of combustion and the ignition process

under SMOC conditions (i.e. steam moderated oxy-fuel combustion) with respect to combustion under an atmosphere of O_2/N_2 , however, Lei K. et al. [37] studied the differences in combustion performed under conventional oxy- fuel conditions (O_2/CO_2). In this study a high-speed chamber that recorded the entire combustion process were used. When N_2 were replaced by steam, they found that:

(i) The ignition process occurs before, according to Zou C et al. [33], Cai L. et al [35] and Liang et al. [36]. All of them attributed this effect to the products of the gasification reaction and WGS reaction (CO and H_2), which benefit the ignition process.

(ii) At low O_2 concentration (<30%) the particle temperature was lower than in O_2/N_2, while at 40% O_2 the temperature in H_2O is higher. They concluded that, at low O_2 concentration the effect of heat capacity and the emissivity of the steam is greater, while at high O_2 concentration this effect decreases, and oxidation causes a greater effect [35].

On the other hand, according to the Marek et al. [31] and Roy et al. [32], the results indicated that, when the combustion atmosphere was O_2/H_2O instead O_2/CO_2, the maximum particle temperature was higher.

Table 2.5 Operating condition, equipment and techniques used by the authors that studied the effect of partial substitution of CO_2 by steam on combustion characteristics

OXY-RFG WET

Ref.	Type of reactor	Reaction condition	Fuel	Conditions studied	Techniques	Measurements
J.Riaza et al.[28]	Entrained flow reactor	$D_{chamber}$=40 mm $L_{chamber}$=1700 mm $T_{combustion}$ t_{est}=1000ºC $T_{ignition}$ t_{est}=400-800ºC (HR 15ºC/min) T_{steam}=250ºC tR=2,5 s	Bituminous coal Anthracite coal d_p=75-150 μm	O_2/N_2, $[O_2]$:21% O_2/CO_2, $[O_2]$:21%, 30%, 35% $O_2/CO_2/H_2O$, $[O_2]/[CO_2]$: 21%/69%, 30%/60%, 35%/55% and 21%/59%, 30%/50%, 35%/45% $O_2/N_2/H_2O$, $[O_2]/[N_2]$:21%/69%, and 21%/59%	High speed camera Two color pyrometer	Ignition Burnout
B.Roy et al. [32]	Fluidized bed	Quartz sand d_{bed}=106-150 μm u_{mf}=0,05 m/s	Victorian brown coal d_p=8-10 mm d_{pchar}=5-6 mm	O_2/CO_2, $[O_2]$:5%,10%,15% a Tb=890ºC O_2/CO_2, $[O_2]$:10% a Tb=925ºC $O_2/CO_2/H_2O$, $[O_2/H_2O]$: 5%/15% (Tb=880ºC), 10%/15% (Tb=885ºC), 15%/15% (Tb=890ºC)	Thermocouple	Particle temperature Carbon consumption rate

Table 2.5 Operating condition, equipment and techniques used by the authors that studied the effect of partial substitution of CO_2 by steam on combustion characteristics (cont).

Ref.	Type of reactor	Reaction condition	Fuel	Conditions studied	Techniques	Measurements
E. Marek [31]	Horizontal furnance	T=950ºC	Two bituminous coals	O_2/N_2, $[O_2]$:21%,35%	Thermocouple	Observation of the ignition and combustion
			Lignite coal	O_2/CO_2, $[O_2]$:21%, 35%	High speed camera	Particle temperature
			L= 2 mm (cubical shape)	$O_2/CO_2/H_2O$, $[O_2]/[CO_2]$: 21%/64%, 21%/54%, 21%/44%		
M.V. Gil [29]	Thermogravimetric analyzer	HR=15 ºC/min ΔT=25-1000ºC Fg=150 cm^3/min	Anthracite coal	O_2/N_2, $[O_2]$:21%	TGA	$T_{ignition}$
			Semi-anthracite coal	O_2/CO_2, $[O_2]$:21%, 30%, 35%		Peak temperature
			Medium-volatile bituminous coal	$O_2/CO_2/H_2O$, $[O_2]/[CO_2]$: 21%/69%, 30%/60%, 35%/55% and 21%/59%, 30%/50%, 35%/45%		Burnout temperature
			high-volatile bituminous coal Biomass (olive waste) d_p=75-150 μm			Maximum and average rate of mass lost

Table 2.5 Operating condition, equipment and techniques used by the authors that studied the effect of partial substitution of CO_2 by steam on combustion characteristics (cont).

Ref.	Type of reactor	Reaction condition	Fuel	Conditions studied	Techniques	Measurements
B. Yi et al. [30]	Thermogravimetric analyzer	HR_1=10 ºC/min	Three ranks of Chinese coal	O_2/CO_2, [O_2]:10%, 21%, 30%, 40%		Tignition
		ΔT=25-150ºC	d_p=45-75 μm	$O_2/CO_2/H_2O$, [O_2]/[H_2O]: 10%/10%, 21%/10%, 30%/10%, 40%/10%; 10%/20%, 21%/20%, 30%/20%, 40%/20%; 10%/30%, 21%/30%, 30%/30%, 40%/30%; 10%/40%, 21%/40%, 30%/40%, 40%/40%	TGA	Peak temperature
		HR_1=20 ºC/min				Burnout temperatura
		ΔT=150-900ºC				Maximum and average rate of mass lost
Cai L. et al [35]	Drop-tube furnance	$D_{chamber}$=10 mm	Bituminous coal	O_2/CO_2, [O_2]: 21%, 30%, 40%	High-speed camera	Ignition distance
		T=1100ºC T_{steam}=150ºC	d_p=97-105 μm	$O_2/CO_2/H_2O$, [O_2]/[H_2O]: 21%/5%, 30%/5%, 40%/5%; 21%/10%, 30%/10%, 40%/10%; 21%/20%, 30%/20%, 40%/20%; 21%/30%, 30%/30%, 40%/30%	Two-color pyrometer	
		Fg_1=1 L/min Fg_2=9 L/min			CFD model	

Table 2.6 Operating condition, equipment and techniques used by the authors that studied the effect of total substitution of CO_2 by steam on combustion characteristics

OXY-STEAM

Ref.	Type of reactor	Reaction condition	Fuel	Conditions studied	Techniques	Measurements
Chun Zou et al. [34]	Drop-tube furnance	$D_{chamber}$=10 mm T=1100ºC Fg_1=1 L/min Fg_2=9 L/min T_{steam}=150ºC	Bituminous coal d_p=97-105 µm	O_2/N_2, [O_2]:21%-50% O_2/H_2O, [O_2]:21%-50%	High-speed camera Two-color pyrometer CFD model	Dynamic behaviour of ignitions Particle temperature Ignition delay ratio
Liang Zhang et al. [36]	Thermogravimetric analyzer	ΔT=25-1000ºC F_g=0,1L/min	Char fom bituminous coal Char from meager coal d_p= 45-75µm	O_2/N_2, [O_2]:21%-40% (HR=20 K/min) O_2/H_2O, [O_2]:21%-40% (HR=20 K/min) O_2/H_2O, [O_2]:21% (HR=10, 15, 20, 25 K/min)	TGA	Tignition Peak temperature Burnout temperature Maximum and average rate of mass lost
Chun Zou et al. [33]	Thermogravimetric analyzer	ΔT=25-900ºC F_g=0,1L/min	Meager coal Bituminous coal d_p= 45-75µm d_p= 75-130µm d_p= 130-150µm	O_2/N_2, [O_2]:21%-40%, 80% (HR=20 K/min) O_2/H_2O, [O_2]:21%-40%, 80% (HR=20 K/min) O_2/H_2O, [O2]:21% (HR=10, 30 K/min) O_2/H_2O, [O2]:21% (HR=20 K/min, 3 d_p)	TGA	Tignition Peak temperature Burnout temperature Maximum and average rate of mass lost

Table 2.6 Operating condition, equipment and techniques used by the authors that studied the effect of total substitution of CO_2 by steam on combustion characteristics (cont.).

Ref.	Type of reactor	Reaction condition	Fuel	Conditions studied	Techniques	Measurements
Lei K. et al. [37]	Drop-tube furnance	T=1000ºC	Bituminous coal	O_2/N_2, $[O_2]$:21%, 30%, 40%	High-speed camera	Particle temperature
		D_{tube}= 5 cm	Biomass (pine sawdust)	O_2/CO_2, $[O_2]$:21%, 30%, 40%	Two-color method	
		L_{tube}= 80 cm	d_p= 75-100μm	O_2/H_2O, $[O_2]$:21%, 30%, 40%		

4. Summary and analysis

The studies reviewed have worked with steam concentration in the range of 5%-80%, in different gas atmospheres and using various equipment and technology (Table 4).

Table 2.2 Summary of the steam concentrations studied, and the technology used in each case. FB: Fluidized bed; TGA: Thermogravimetric Analyzer; ER: Entrainer reactor; DTF: Drop tube furnace; HF; Horizontal furnace

Conditions				Technology
[O_2]	**[N_2]**	**[CO_2]**	**[H_2O]**	**Reactor**
5%		80%	15%	FB
10%		75%	15%	FB
		80%	10%	TGA
		70%	20%	TGA
		60%	30%	TGA
		50%	40%	TGA
15%		70%	15%	FB
21%		74%	5%	DTF
	69%		10%	ER
	59%		20%	ER
			79%	DTF/TGA
		69%	10%	ER/TGA/DTF
		64%	15%	ER/HF
		59%	20%	ER/TGA/DTF
		54%	25%	HF
		49%	30%	TGA/DTF
		44%	35%	HF
		39%	40%	TGA
30%			70%	DTF/TGA
		65%	5%	DTF
		60%	10%	ER/TGA/DTF
		55%	15%	ER
		50%	20%	ER/TGA/DTF
		40%	30%	TGA/DTF
		30%	40%	TGA
35%		55%	10%	ER/TGA
		50%	15%	ER
		45%	20%	ER/TGA
40%			60%	DTF/TGA
		55%	5%	DTF
		50%	10%	TGA/DTF
		40%	20%	TGA/DTF
		30%	30%	TGA/DTF
		20%	40%	TGA
50%			50%	DTF
80%			20%	TGA

All the authors came to the following conclusions:

I. Higher O_2 concentration in the combustion atmosphere causes: (i) an advance in ignition of both volatile and char particle, (ii) higher particle temperature and (iii) higher reaction rate of the coal particle. These results indicate that the combustion process is strongly influenced by the O_2 diffusion through the particle gas boundary layer.
II. The coal combustion rate is higher in low-range coals compared to higher-range coals, due to their higher reactivity.
III. The coal particle temperature is always higher in the presence of steam compared to that obtained in oxy-CO_2. This effect is attributed to the combustion of products generated by the steam gasification reaction (CO and H_2).
IV. The authors who tested at low vapor concentrations (<20%) found no significant differences on the coal combustion rate [28,29], however, when higher concentrations of H_2O [30] are used, the reaction rate seems to be increased.

However, in reference to the ignition time (homogeneous and heterogeneous) in the presence of steam, contradictory results were found.

According to the literature, steam could produce the following effects:

I. **Specific heat**. The higher heat sink (kJ/(m^3K)) of steam compared with N_2 (Table 2.1) could reduce the coal particle temperature and therefore, the combustion rate and the ignition delay are reduced. Similarly, the lower heat sink of steam in comparison to that of CO_2 could result in an increase in the fuel temperature and combustion rate.
II. **The steam gasification reaction** (Reaction 1). This endothermic reaction can reduce the temperature of the particle and its contribution could increase the rate of char conversion.
III. **The oxidation reaction of H_2 and CO.** The steam gasification reaction and the WGS reaction produce a large amount of H_2 and CO, whose oxidation could produce an increase in particle temperature.
IV. **The radiant properties of gases**. A high steam concentration in gases lead to an increase in the rate of radiant heat transfer due to the high emissivity of the steam, which could result in a reduction in particle temperature compared to that found in combustion with O_2/N_2 and O_2/CO_2 [28].
V. **Diffusivity**. The diffusion coefficient of O_2 in H_2O is higher than in N_2 and in CO_2 (Table 2.1), so the collision probability of O_2 in the particle surface is much higher in H_2O, which would contribute to an increase in combustion rate and particle temperature.

In order to visualize the ignition results, an ignition delay ratio (IDR) has been calculated in this work, according to (2.1). This parameter relates the start of the ignition process, either in terms of temperature, distance or time, in an atmosphere with presence of steam, relative to a base case in which steam is not present. The calculated ignition delay ratio is shown in Figure 2.5. This ratio has been applied to all the ignition experiments, reviewed in this work, that have been carried out at 21% in O_2 by varying the steam concentration in different combustion atmospheres.

$$IDR = \frac{P_{H_2O}}{P_{BASE}} \qquad (2.1)$$

Where P_{H2O} is the ignition parameter (temperature, time or ignition point) in the presence of steam and P_{BASE} is the ignition parameter for the base case, when steam is not present. Therefore, if *IDR>1* ignition will be delayed in the presence of steam and if *IDR<1,* the ignition will be advanced when the steam participates in combustion reaction.

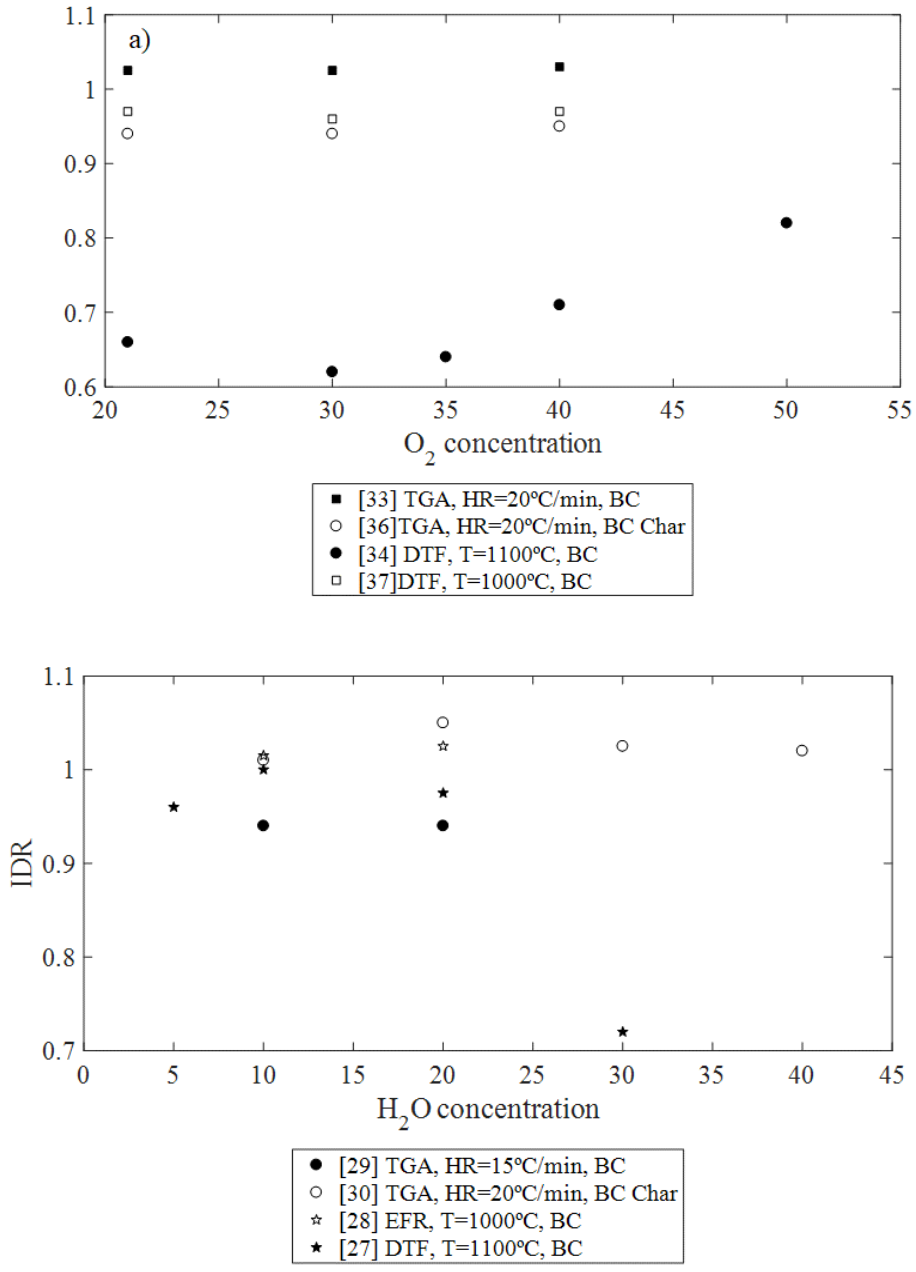

Figure 2.5 Ignition delay ratio for different vapor concentrations in mixtures of O_2/H_2O vs O_2/N_2 (a) and $O_2/CO_2/H_2O$ vs O_2/CO_2 (b) with a concentration of O_2 of 21%, calculated from the results of the revised literature. DTF: Drop tube furnace; EFR: Entrained Flow reactor: BC: Bituminous coal; BC-char: Bituminous char

All results obtained in DTF [34,37] are similar, showing that the coal particles ignition in the presence of steam occurs slightly earlier than in O_2/N_2 and O_2/CO_2 atmospheres. When the experiments are carried out in TGA [27,36], coal ignition is slightly delayed for the same conditions, which can be related to the differences in the heating rate. Nevertheless, the IDR is in all cases very close to 1 except in cases where the operating temperature is greater than 1000ºC and the vapor concentration is greater than 20%. At these conditions it is possible that the gasification reactions have a greater influence and probably due to this fact the ignition stage is brought forward.

Chapter 3. Experimental

In this chapter the experiments carried out to measure the combustion characteristics (i.e. particle temperature and conversion), at high O_2 concentration, as well as the calibration of the digital camera, required to execute the temperature measurements, are described.

It is important to note that in previous works identical combustion experiments were carried out, both for the calibration of the digital camera and for the study of the effect of CO_2, under different conditions (i.e. concentrations of O_2 below 40% in the combustion tests and calibration of the pyrometric technique until 1020ºC) [26]. At higher concentrations the measurement technique was not valid (the method is saturated when the temperature reached by the particle is higher than 1020ºC). Therefore, to measure the fuel temperature using higher oxygen concentrations, new calibration tests are needed. In order to mitigate the radiation, in the visible spectrum, that reaches the sensor, this calibration tests were performed using a neutral density filter situated on the camera lens.

1. Oxy-fuel combustion experiments

A summary of the description and characteristics of the experiments performed is shown in Table 3.1. The results of the combustion experiments shown in Chapter 4 are the average of six tests carried out under the same conditions, also, in each test, numerous temperature values of the char particles were recorded. Therefore, the results can be considered representative.

Table 3.1 Experimental and theoretical studies carried out in this master thesis.

tudy	Influence of CO_2 concentration of the char conversion during oxy-fuel combustion in a fluidized bed
Description	Combustion of a single spherical char particle during its combustion in FB (2D)
Type of reactor	Bubbling fluidized bed
Reaction condition	$T_{furnace}$=800ºC
Fuel	Beech wood char (d_p=8 mm)
Conditions studied	O_2/N_2 atmosphere (11%-100% O_2) O_2/CO_2 atmosphere (11%-100% O_2)
Techniques	Digital camera (P1C)
Measurements	Temperature of the char particle surface and burnout time

1.1 Preparation of char particles

The production of char particles used in this work were obtained from Beech wood (Figure 3.1). The immediate analysis of this fuel is presented in Table 3.2.

The wood particle was heated inside an electric furnace from room temperature until it reaches 800 ºC. A low heating rate (10 ºC/min) was used in order to reduce the char fragmentation during the devolatilization of biomass. The particles are located inside a closed ceramic crucible, in order to avoid the contact of char with oxygen during devolatilization. Although combustion of the particle surface may occur with the oxygen existing inside the crucible before closing, this layer is removed during the shaping process of the char. Each char particle was shaped into a spherical or rectangular form, whose weights and sizes were fixed according to the tests where they were used. All rectangular char particles were drilled on their surface to make a gap (0.5 x 0.8 x 4 mm) to embed a K-type thermocouple in it (Figure 3.6).

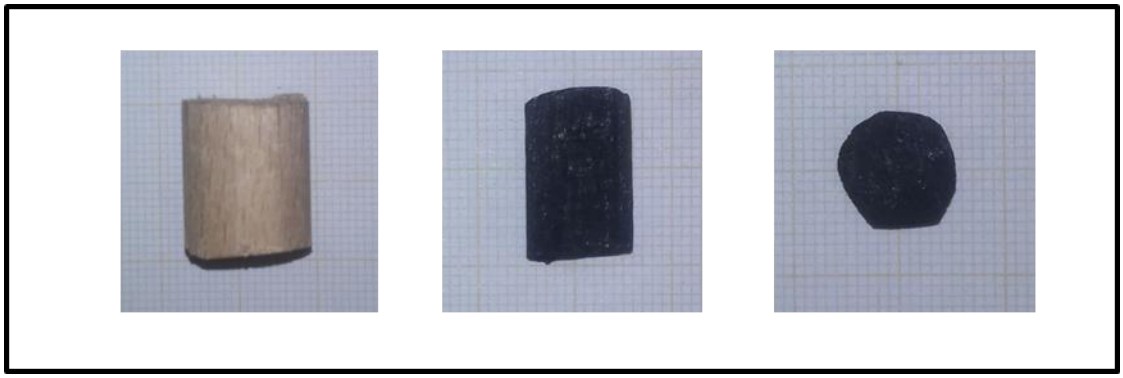

Figure 3.1 Beech wood char particle

Table 3.2 Beech wood properties.

Immediate analysis, % (Beech wood char)	
Moisture	8.10
Ash	0.63
Volatile	84.86
Fixed Carbon	14.52

1.2 Experimental set-up

A Fluidized bed (FB) reactor (lab scale), built in 310 steel, was used in this work, shown in Figure 3.2. The FB reactor has a quartz window in the bottom part (18 x 21 x 0.5 cm) that allows direct visual observation of the bed and optical measurements. The geometry of the reactor is two-dimensional (22 cm x 50 cm x 1.8 cm) in order to obtain as many images of the char particle as possible.

The reactor is in the center of an electric furnace (rectangular high-temperature hearth: 50 x 70 x 30 cm) and welded to the collector. The furnace also has a quartz window (18 x 18 x 0.5 cm) to allow the visibility of the particle during combustion and it is equipped with a surface that homogenizes the temperature and radiation from resistances (11KW). This homogenizing surface consists of a 310 steel sheet with ideal blackbody behavior (painted with 1050ºC resistant black paint).

A digital camera JVC Everio HD (CMOS sensor of 2 Mpxs) was used to capture the thermal radiation located at a working distance (WD) of 100 cm, with a field of view of 24º (FOV), that it was maintained constant in all experiments.

Silica sand served as bed material (320-500 µm), whose height at rest was 8 cm (~300 g). The bed temperature was controlled by a thermocouple (0.15 cm sheath diameter) immersed in the bed and connected to the electric oven using a PID controller.

All tests were carried out in a darkroom in order to only allow radiation from the char and from the background to reach the sensor [52]. The main characteristics of the experimental set-up are shown in Table 3.3.

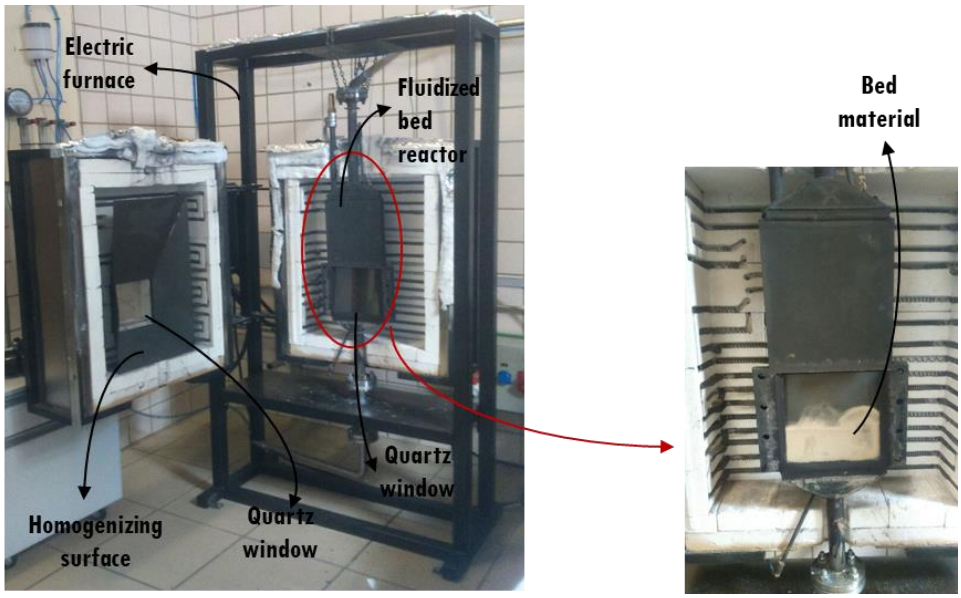

Figure 3.2 Experimental set-up

Table 3.3 Experimental set up

Equipment	Information
Electric furnace	Electric power: 11KW High temperature hearth: 50 cm x 70 cm x 30 cm Window: 19.5 cm x 19.5 cm
Fluidized bed reactor	22 cm x 30 cm x 1,8 cm (Top) 28 cm x 20 x 1,8 cm (Bottom) 310 steel Bed of silica sand, d_i: 0.32-0.5 mm U_{mf}: 0.18 m/s (25ºC)
Digital camera	JVC Everio 2 Mpxs WD (100 cm), FOV (24°)

1.3 Experimental methodology

The experimental configuration to perform the combustion tests is shown in Figure 3.3. Combustion tests were carried out using 8 mm diameter beech wood char. The fluidization agent used was a mixture of O_2/N_2 (combustion tests) and O_2/CO_2 (oxy-combustion tests) at O_2 concentrations of 11% to 100% O_2.

Table 3.4 Operation conditions in the experimental tests.

Operating condition studied	
O_2 concentration	40%, 50% 60% 70% 80%, 100%
Particle diameter	8 mm
Furnace temperature	800ºC
Bed material	
Particles diameter	320-500 µm
Fluidization velocity	2 U_{mf} (0.36 m/s)
Bed height	8 cm

The digital camera records the particle during its conversion, from the start of combustion (when the particle is introduced into the reactor) to the end of the reaction (when the particle is not visible). These videos are separated into frames (images) using an image processing software (Adobe Premier Pro SC6).

When the images of the combustion test have been generated, those which allow the suitable measurement of surface temperature (clear images) of the char are selected. The selection criterion is explained in detail in Appendix I.

The interpretation of the images (temperature reached by the particle in the selected frame) is carried out using a Matlab code performed during previous work by Salinero et al. [49,50].

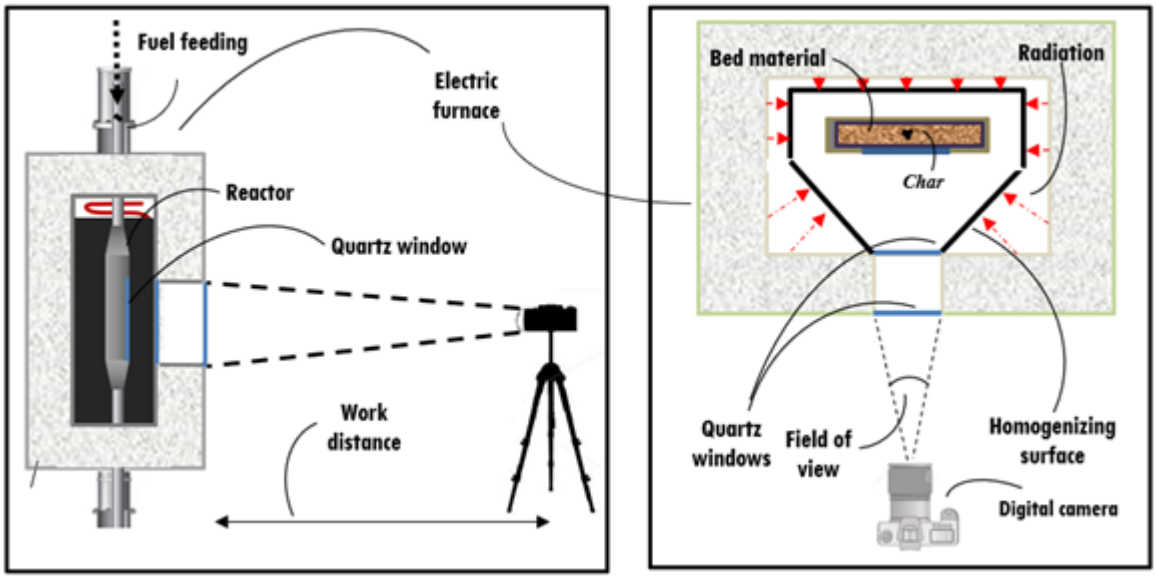

Figure 3.3 Experimental set up in combustion tests

2. Calibration of the digital camera

Temperature measurement by pyrometry is based on the capture and interpretation of thermal radiation emitted from a body whose temperature is to be measured. This thermal radiation can be captured and interpreted by a standard digital camera, if this radiation includes the visible spectral band.

The digital camera separates the light that the sensor receives into three spectral bands or colors: red (0.62-0.7 μm), green (0.49-0.58 μm) and blue (0.45-0.49μm). When radiation reaches the sensor, each pixel generates three values known as digital numbers that measure the radiation belonging to each spectral band [52]. Using a processing image software, three matrices for each image are obtained, where each element (m,n) contains the digital number associated with the radiation received from the scene (Figure 3.4).

A sensor has a lower limit of energy level (W/m^2) and for radiation below this limit, the digital number assigned by a pixel is null. The sensor also has a upper limit of energy level above which the pixel becomes saturated and a maximum value is assigned (saturation) [49].

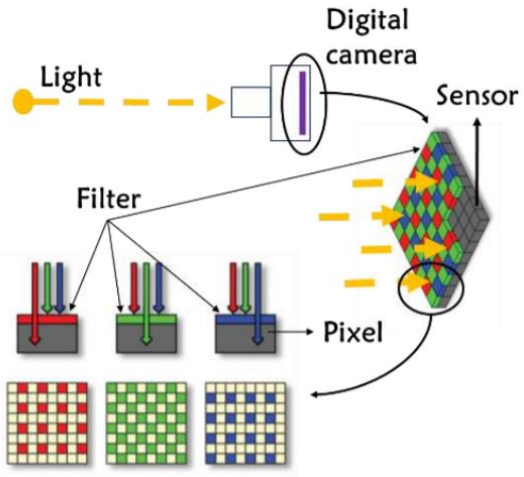

Figure 3.4 Capture and interpretation of the radiation from the viewed scene by the digital camera [49].

Char particle temperature can be measured by pyrometry using simultaneously the information contained in two different visible spectral bands or colors. This application, named two-color pyrometry (P2C) allows calculating the temperature by:

$$T_{P2C,i/j} = \frac{C_2\left(\frac{1}{\lambda_j}-\frac{1}{\lambda_i}\right)}{\left(\ln\left(\frac{DN_i}{DN_j}\right)+\ln(\beta_{i/j})\right)-5\ln\left(\frac{\lambda_j}{\lambda_i}\right)}. \quad (3.1)$$

where λ is the average wavelength within the visible spectral region in which the digital number (DN) is calculated (indexes "i" and "j" can be equal to "r", "g", or "b" from the red, green or blue spectral band, respectively); C_2 is the second Planck's constant; and $\beta_{i/j}$ is a calibration parameter that will be described below.

If the surface emissivity is known and the digital numbers are used sequentially, the range of temperature that can be measured and its accuracy are improved compared with the traditional P2C [49], and the temperature can be calculated by:

$$T_{P1C} = \frac{C_2}{\lambda_k\left[\ln\left(\Phi_k\,\frac{\varepsilon_{rs}(\lambda,T)\,C_1}{\lambda_k^5}\right)-(\ln(\beta_k)+\ln(DN_k))\right]} \quad (3.2)$$

The advantage of this technique during measurements of char temperature in FB combustion experiments is discussed has been discussed [49,50,51]. This approach is the one used in the present work and named one-color pyrometry (PC1).

To apply P2C (3.1) and P1C (3.2) to obtain the viewed scene temperature whose radiation is captured and interpreted the value of the calibration parameter β ($\beta_{P2C,\,ij}$ and $\beta_{P1C,\,k}$) is needed. These parameters lump the optical and electronic configurations of the experimental set-up, as well as the hypothesis and simplification of the heat transfer model [50].

Therefore, to apply this measurement technique a previous calibration of the digital camera is required. Such calibration is carried out in three steps: (i) experimental determination of the DNk-T curves; (ii) calculation of the empirical parameter β_k and; (iii) validation of the method. The two last steps are detailed in Appendix V.

The experimental configuration to perform the calibration tests is shown in Figure 3.5. The temperature inside the furnace is maintained at 800ºC (±1ºC) or 900ºC (±1ºC) depending on the test. A thin and flexible K-type thermocouple (500 mm sheath diameter) is placed inside the surface gap as shown in Figure 3.6 Thus, the temperature measured by the thermocouple is the surface temperature of the particle that surrounds the thermocouple during combustion.

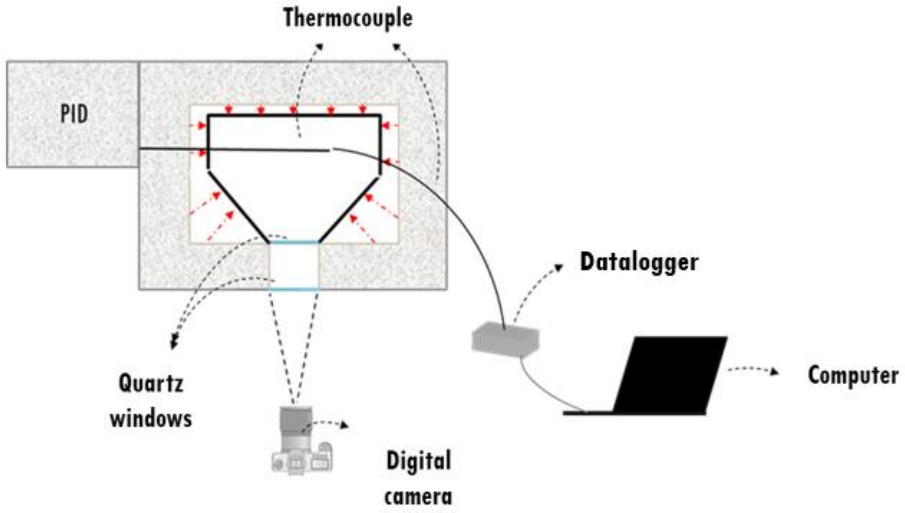

Figure 3.5 Experimental set up in calibration tests

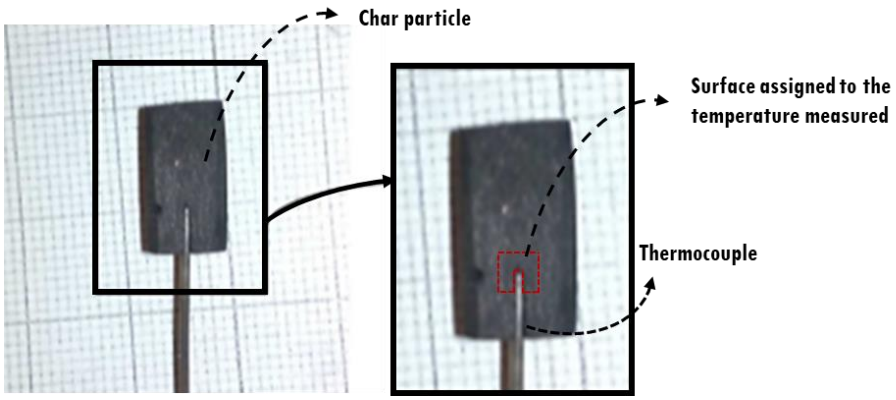

Figure 3.6 Char particle ready for a calibration test.

The optical and electronic parameters of the digital camera (zoom, focus, distance) are adjusted before each test and the test is performed in a darkroom.

The combustion of a rectangular beech wood char particle was carried out in each test. The particle is placed in the center of the furnace at operating temperatures of 800ºC and 900ºC and O_2 concentration (in N_2) from

0 to 100%. In this way, the combustion temperatures of the char particles covered suitable temperature range to analyze the combustion/oxy-fuel combustion of a single char particles in FB reactor. More details about this methodology are explained in [49, 50].

Table 3.5 Calibration experiments

Tests	$T_{furnace}$	$[O_2]$	Gas flow
6	800ºC	21%	0 Nm^3/h
2		21%	3 Nm^3/h
2			4 Nm^3/h
4	900ºC	21%	0 Nm^3/h
2		21%	4 Nm^3/h
2		100%	2 Nl/min
5			3 Nl/min
5			4 Nl/min

Chapter 4.
Model development

In order to study the effect of steam in oxy-fuel combustion a theoretical model is developed. The present chapter presents a detailed model to predict the evolution of the temperature and conversion of a char particle under different operating conditions.

1. Modes of conversion of a single char particle

Modeling of the conversion of fuel particles is normally conducted by dividing the process in several steps, drying (the water in the particle starts evaporating), devolatilization (volatiles gases and tars are released from the particle and are combusted in the presence of oxygen) and char conversion (char reacts with gas enviroment, in general, a mixture of oxygen, steam and CO_2 to form to form mainly CO, H_2 and CO_2). The model developed is focused in the last stage (i.e. char conversion).

Depending on reaction conditions and fuel properties, different physical and chemical effects can dominate heterogeneous char conversion and play a rate limiting role. Three different regimes of fuel conversion can be distinguished [57]. In regime I, mass transport processes like internal particle diffusion and external mass transfer are distinctly faster than the heterogeneous reaction. Therefore, reaction is considered the rate limiting step and mass transfer effects can be neglected in modeling approaches. For this case, char conversion proceeds uniformly throughout the entire particle. As a result, the diameter stays constant during reaction and char density decreases linearly with conversion which can be described by the uniform conversion model, UCM (Figure 4.1 a).

In regime III, external mass transfer of gases from the bulk phase to the particle surface is the slowest and thus the rate limiting process. The reaction occurs only at the external surface of the particle, resulting in a constant particle density. As the time progresses, the particle shrinks in size due to the radial movement of the reaction front towards the center of the particle, which can be expressed by means of the shrinking core model (SCM). The shrinking core model can be classified according to the absence (SUPM) or presence (SUCM) of an ash layer surrounding the shrinking unreacted core (Figure 4.1 b and c).

Lastly, regime II is dominated by the combination of both, reaction and intra particle diffusion. Carbon consumption inside the particle is non-uniform, meaning that diameter as well as density change during conversion (Figure 4.1 d and e).

Case (a), (b) and (c) are the classical models, representing extreme behavior, whereas cases (d) and (e) represent more general mode of char conversion. The difference between PMSP and PMSC models is in the behavior of the ash, which is rapidely (attrition time scale is much lower than the time scale of char conversion) removed by attrition in the case of the PMSP, whereas it remains attached in the PMSC during the weole conversion process. The same extreme cases with regard to the ash are considered in models PM d and e: it is fastly removed in the PMSP, whereas it is maintained in the PMSC.

In this work a one-dimensional detailed particle simulation model is developed describing intra particle transport phenomena and heterogeneous char combustion and gasification reactions following an improved version of PMSC as explained below.

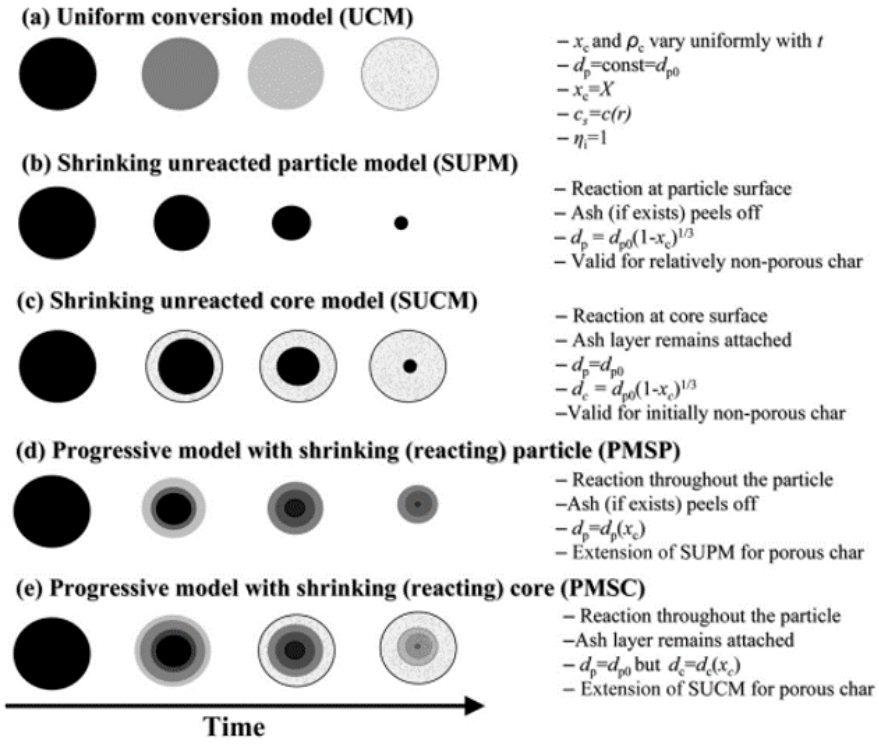

Figure 4.1 Single char-particle conversion model [56]

2. Modelling approach

The problem under study is a char particle, located in a fluidized bed, initially exposed to a given oxidative environment with specified composition and temperature (Figure 4.2). The different reaction atmosphere studied are: O_2/N_2 (air combustion case), O_2/CO_2 (oxy-fuel with dry recycle case), $O_2/CO_2/H_2O$ (oxy-fuel with wet recycle case) or O_2/H_2O (oxy-steam case). The assumptions made are summarized as follows:

i. The char particle is spherical and only one dimension is considered.
ii. The gases behave as ideal gases.
iii. The composition of the bulk gas is constant.
iv. The ash is kept attached to the particle until some time, beyond which the ash is detached. The rate of external char layer movement is calculated by assuming that the local external char (ash with some remaining carbon) is instantaneously detached once a prefixed local conversion threshold is reached.
v. The homogeneous reaction of CO, taking place outside of the particle, in not considered. This assumption is reasonable for large particles burning in a fluidized bed at atmospheric pressure and temperature below 1000ºC. Inert material provides a CO oxidation quenching effect in these conditions [58].
vi. Gas velocity inside the particle is small and the convective term is insignificant regarding diffusion term.

3. Model description and formulation

In order to describe the kinetic model, char gasification and combustion reaction and transport equation are shown below as well as the formulation for the implementation in Matlab.

3.1 Char gasification and combustion

The consumption of a char particle is given by oxidation [60]:

$$C(s) + \frac{2+\alpha/\beta}{2(1+\frac{\alpha}{\beta})} O_2(g) \rightarrow \frac{\alpha/\beta}{(1+\frac{\alpha}{\beta})} CO(g) + \frac{1}{(1+\frac{\alpha}{\beta})} CO_2(g) \quad \text{R.1}$$

and gasification

$$C(s) + CO_2(g) \rightarrow 2CO(g) \quad \text{R.2}$$

$$C(s) + H_2O(g) \rightarrow CO(g) + H_2(g) \quad \text{R.3}$$

Reaction R.1 is exothermic, whereas reactions R.2 and R.3 are endothermic. α and β are mechanism coefficients. When α=0 means that CO_2 is the primary product of combustion, whereas CO is the primary combustion product when β=0. Arthur [61] proposed a kinetic equation to estimate the produced ratio α/ β, i.e. the molar ratio CO/CO_2:

$$\frac{\alpha}{\beta} = A_{CO/CO_2} \exp\left(-\frac{E_{CO/CO_2}}{R_g T_C}\right) \quad (4.1)$$

3.2 Transport equations

The mass conservation of char is described as:

$$\frac{\partial \rho_c}{\partial t} = -\left(R_{v,O_2} + R_{v,CO_2} + R_{v,H_2O}\right) \quad (4.2)$$

where R_{v,O_2}, R_{v,CO_2} and R_{v,H_2O} are the rates of char combustion and gasification. They are assumed to follow the following kinetics ([73]):

$$R_{v,O_2} = A_{O_2} s \, exp\left(-\frac{E_{O_2}}{R_g T_p}\right) Y_{O_2} \quad (4.3)$$

$$R_{v,CO_2} = \rho_{CO_2} A_{CO_2} s \, T \, exp\left(-\frac{E_{CO_2}}{R_g T_p}\right) Y_{CO_2} \quad (4.4)$$

$$R_{v,H_2O} = \rho_{H_2O} A_{H_2O} \, s \, T \, exp\left(-\frac{E_{H_2O}}{R_g T_p}\right) Y_{H_2O} \quad (4.5)$$

where "s" is the reaction surface at time t per unit of volume. During combustion, the available surface area is changing (from s_0 at t=0) with the change of carbon conversion degree x_c and it is estimated based on the Random Pore Model (RPM) proposed by Bhatia and Perlmutter [66].

$$s = s_0(1 - x_c)(1 - \psi \ln(1 - x_c))^{1/2} \quad (4.6)$$

This model introduces a structural parameter ψ by considering that the char particle is porous, and the reaction takes place at the internal surface of the pores. As the reaction proceeds, a random overlapping of the pores occurs which can increase or reduce the re-active surface area. [67]

This model is one of the main structural models applied to char gasification kinetics [56]. Magnaterra et al. [68] found that the Random Pore Model satisfactorily fitted the reaction rate of char combustion, assuming a structural parameter $\psi = 2.6$ for beech wood char particles.

The molar fraction of each gaseous species (i) can be obtained from the following molar transport equation valid for the particle:

$$\frac{\partial \varepsilon_p \rho_g Y_i}{\partial t} = \frac{1}{r^k} \frac{\partial}{\partial r}\left(r^k \rho_g D_{eff,i} \frac{\partial Y_i}{\partial r}\right) + S_{m,i} \quad (4.7)$$

where $i = O_2, CO_2, CO, H_2O, N_2, H_2$ and k=2 (sphere)

The three terms in this equation represent the temporal change of concentration, the diffusive flux and a source term due to heterogeneous reactions. Y_i denotes the molar fraction of species i and $D_{eff,i}$ is the effective diffusion coefficient of species i in a multi component gas mixture. The source terms in (4.7) are calculated as follows:

$$S_{m,O_2} = -R_{v,O_2} \tag{4.8}$$

$$S_{m,CO_2} = \frac{2\beta}{\alpha+2\beta} R_{v,O_2} - R_{v,CO_2} \tag{4.9}$$

$$S_{m,CO} = \frac{2\alpha}{\alpha+2\beta} R_{v,O_2} + 2R_{v,CO_2} \tag{4.10}$$

$$S_{m,H_2O} = R_{v,H_2O} \tag{4.11}$$

$$S_{m,N_2} = 0 \tag{4.12}$$

The effective diffusivity of the gas species in the solid is calculated as [45]:

$$D_{eff,i} = \frac{\varepsilon_p}{\tau} D_i \sim {\varepsilon_p}^2 D_i \tag{4.13}$$

where ε_p is the internal porosity of char and τ is the pore tortuosity. Diffusivity of the gases was determined using the multicomponent diffusion coefficient expression developed by Fairbanks and Wilke [75]:

$$D_i = \frac{1-Y_i}{\sum_{j=i}^{N} \frac{Y_j}{D_{i,j}}} \tag{4.14}$$

This expression assumes the diffusion of one gas into a mixture of stagnant gases, therefore, it is reasonable to apply it in the cases where N_2 is the main component of the gas mixture, but questionable when CO_2 (or H_2O) is the main fluidization agent. However, in order to simplify the model, (4.14) is applied to all the cases.

On the other hand, the heat conservation of char particle is given as:

$$\frac{\partial((1-\varepsilon_p)\rho_p C_p T_p)}{\partial t} = \frac{1}{r^k}\frac{\partial}{\partial r}\left(\lambda r^k \frac{\partial T_p}{\partial r}\right) + Q \tag{4.15}$$

Where $i = O_2, CO_2, CO, H_2O, N_2, H_2$ and k=2 (sphere)

The first term represents the temporal change in particle temperature and second term represents the conduction heat transfer through the particle. The source of heat Q is the heat of heterogeneous reactions (combustion and gasification):

$$Q = R_{v,O_2}\Delta H_1 + R_{v,CO_2}\Delta H_2 + R_{v,H_2O}\Delta H_3 \tag{4.16}$$

3.3 Boundary conditions: heat and mass fluxes

To solve Eq. 14 numerically, boundary conditions at the particle center and at the outer surface need to be formulated. In consequence of assuming symmetric particles, at r = 0 the gas flux of each species and the intraparticle heat flux is set to zero (4.17).

$$\left.\frac{\partial T}{\partial r}\right|_{r=0} = \left.\frac{\partial Y_i}{\partial r}\right|_{r=0} = 0 \tag{4.17}$$

At the external surface of the particle, at r = R, the diffusive flux of each gaseous species has to be equal to the external mass transfer, defined by the product of the mass transfer coefficient $h_{m,i}$ and the concentration difference between the particle surface and the surrounding gas phase (4.18).

$$-D_i \frac{\partial Y_i}{\partial r}\Big|_{r=R} = h_{m,i}(Y_{i,s} - Y_{i,\infty}) \quad (4.18)$$

The diffusion rate coefficient, $h_{m,i}$, is calculated by

$$h_{m,i} = \frac{Sh_{b,i} D_{eff,b}}{d_p} \quad (4.19)$$

where d_p represents the diameter of the char particle, Sh is the Sherwood number (Table 4.3) and $D_{eff,b}$, the effective diffusivity in the bed, which is determined as:

$$D_{eff,b} = \frac{\varepsilon_b}{\tau_b} D_i \quad (4.20)$$

where ε_b and τ_b are the porosity and tortuosity of the bed material respectively.

The intraparticle heat flux at the outer surface can be calculated as:

$$-\lambda_p \frac{\partial T}{\partial r}\Big|_{r=R} = h_{conv}\,(T_{p,s} - T_\infty) + e_{eff}\sigma\,(T_{p,s}^4 - T_b^4) \quad (4.21)$$

The first term on the right-hand side represents the rate of heat transfer due to convection between particle and gas and the second one is the heat transferred between the particle and the bed material due to the radiation.

The convective heat transfer coefficient between gas and particle in fluidized beds is calculated as:

$$h_{conv} = \frac{Nu_b \lambda_g}{d_p} \quad (4.22)$$

Where Nu_b represents the Nusselt number and it is calculated as shown in Table 4.3.

e_{eff} represents the effective emissivity and it is estimated as [65]:

$$e_{eff} = \frac{1}{\frac{1}{e_p} + \frac{1}{e_b} - 1} \quad (4.23)$$

Finally, the initial conditions of the fuel particle are:

$T_p = T_0$, $\rho_p = \rho_0$, $\varepsilon_p = \varepsilon_{p,0}$ at t=0, 0 < r < R

3.4 Discretization and solution

To solve the proposed differencial equations the finite volume method is applied. The main three steps followed for its computer implementation are summarized as follow.

Step 1: Grid generation

The assumed spherical particle is radially discretized in evenly spaced shells. Between each small domain one nodal point is placed (*P*). The boundaries of control volumes are positioned mid-way between adyacent nodes. Thus, each node is surrounded by a control volume or cell (Figure 4.2). A general nodal point *P* is sourrounded by two neighbours *W* (node to the west) and *E* (node to the east). The west side face of the control volume is referred to by *w* and the east side control volume boundary by *e*. The distance between the nodes *W* and *P*, and between nodes P and E are identified by ξ_{PW} and ξ_{PE} respectively.

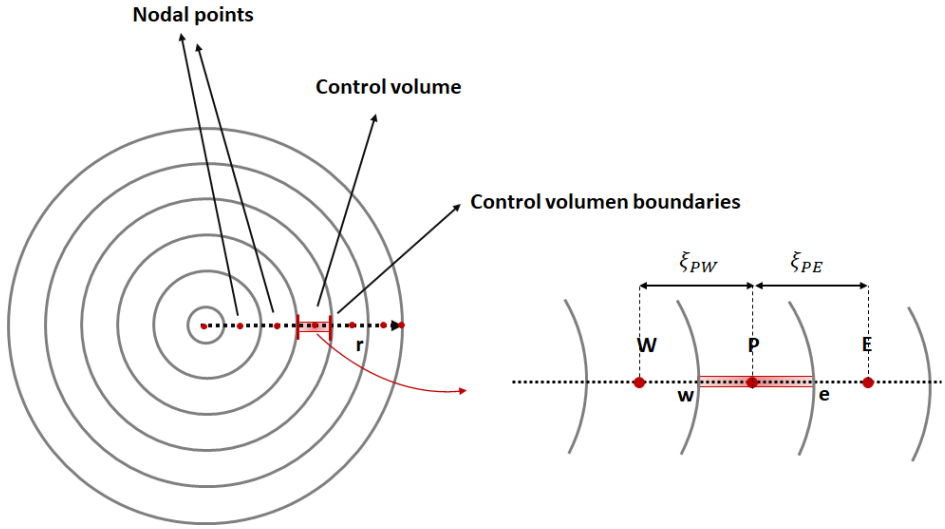

Figure 4.2 Discretization scene of the model

Step 2: Discretization

The key point of the finite volume method is to integrate the equation all over the control volume to yield a discretized equation at its nodal points P. For instance, Eqs. (4.7) and (4.15) integrated for the control volume defined above give the following equations:

$$\int \frac{\partial \varepsilon_p \rho_g Y_i}{\partial t}\, dV = \int \frac{1}{r^2}\frac{\partial}{\partial r}\left(r^2 \rho_g D_{eff,i} \frac{\partial Y_i}{\partial \mathrm{r}}\right) dV + \int S_{m,i} dV \qquad (4.24\ a)$$

$$\int \frac{\partial((1-\varepsilon_p)\rho_p C_p T)}{\partial t} dV = \int \frac{1}{r^2}\frac{\partial}{\partial r}\left(\lambda r^2 \frac{\partial T}{\partial r}\right) + \int Q\, dV \qquad (4.25\ a)$$

Which after integration yields the discretized forms of the equations,

$$\frac{\partial \varepsilon_p \rho_g Y_i}{\partial t}\Delta V = \left(D_{eff,i}\, A \frac{\partial Y_i}{\partial \mathrm{r}}\right)_e - \left(D_{eff,i}\, A \frac{\partial Y_i}{\partial \mathrm{r}}\right)_w + S_{m,i}\Delta V \qquad (4.24\ b)$$

$$\frac{\partial((1-\varepsilon_p)\rho_p C_p T)}{\partial t}\Delta V = \left(\lambda\, A \frac{\partial \mathrm{T}}{\partial \mathrm{r}}\right)_e - \left(\lambda\, A \frac{\partial \mathrm{T}}{\partial \mathrm{r}}\right)_w + Q\Delta V \qquad (4.25\ b)$$

where A is the cross-sectional area of the control volume and ΔV is the volume.

For the calculation of gradients at the control volume faces an approximate distribution of properties between nodal points is used. Linear approximations seem to be the obvious and simplest way of calculing interface values and the gradients (central differencing [77]).

$$D_{eff,iw} = \frac{D_{eff,iW} + D_{eff,iP}}{2} \qquad (4.26\ a)$$

$$D_{eff,ie} = \frac{D_{eff,iP} + D_{eff,iE}}{2} \qquad (4.26\ b)$$

and in the same way:

$$\lambda_w = \frac{\lambda_W + \lambda_P}{2} \qquad (4.27\ a)$$

$$\lambda_e = \frac{\lambda_P + \lambda_E}{2} \qquad (4.27\ b)$$

Second-order schemes are possible to improve the solution but it was not implemented in the present model because the first-order scheme was accurate enough. Finally, the mass and energy conservation equation discretized are given by:

$$\frac{\partial \varepsilon_p \rho_g Y_i}{\partial t}\Delta V = \rho_g \left[D_{eff,ie}\, A_e \frac{Y_{i,E}-Y_{i,P}}{\xi_{EP}} - D_{eff,iw}\, A_w \frac{Y_{i,P}-Y_{i,W}}{\xi_{PW}}\right] + S_{m,i}\Delta V \quad (4.28)$$

$$\frac{\partial((1-\varepsilon_p)\rho_p C_p T)}{\partial t}\Delta V = \lambda_e A_e \frac{T_E-T_P}{\xi_{EP}} - \lambda_w A_w \frac{T_P-T_W}{\xi_{PW}} + Q\Delta V \quad (4.29)$$

where $Y_{i,E}$ and T_E are the molar fraction and particle temperature respectively, calculated in the node to the east. $Y_{i,W}$ and T_W are the same parameters calculated in the node to the weast. $Y_{i,P}$ and T_P represent the concentration and particle temperatura in the evaluated node.

To calculate the mass flow of the gaseous species and particle temperature in r=0 (where there is a singularity), equations (4.7) and (4.15) were solved at r=0 by Taylor expansions of second orders, yielding the following expressions:

$$\frac{\partial \varepsilon_p \rho_g Y_i}{\partial t} = \rho_g D_{eff,i}\left(\frac{2}{r}\frac{\partial Y_i}{\partial r} + \frac{\partial^2 Y_i}{\partial r^2}\right) + S_{m,i} \quad (4.30\text{ a})$$

$$\frac{\partial((1-\varepsilon_p)\rho_p C_p T)}{\partial t} = \lambda\left(\frac{2}{r}\frac{\partial T}{\partial r} + \frac{\partial^2 T}{\partial r^2}\right) + Q \quad (4.30\text{ b})$$

then, by applying boundary conditions in *r=0* (4.17) to (4.30 a) and (4.30 b) it result as:

$$\frac{\partial \varepsilon_p \rho_g Y_i}{\partial t} = 3\,\rho_g D_{eff,i}\frac{\partial^2 Y_i}{\partial r^2} + S_{m,i} \quad (4.31\text{ a})$$

$$\frac{\partial((1-\varepsilon_p)\rho_p C_p T)}{\partial t} = 3\lambda\frac{\partial^2 Y_i}{\partial r^2} + Q \quad (4.31\text{ b})$$

Resulting in a mass and energy conservation equation discretized in *r=0* as:

$$\frac{\partial \varepsilon_p \rho_g Y_i}{\partial t}\Delta V = 3\,\rho_g\left(D_{eff,ie+1}\frac{Y_{i,E+1}-Y_{i,E}}{\xi_{P(E+1)}^{\,2}} - D_{eff,ie}\frac{Y_{i,E}-Y_{i,P}}{\xi_{PE}^{\,2}}\right) + S_{m,i}\Delta V \quad (4.32\text{ a})$$

$$\frac{\partial((1-\varepsilon_p)\rho_p C_p T)}{\partial t}\Delta V = 3\left(\lambda_e\frac{T_{E+1}-T_E}{\xi_{P(E+1)}^{\,2}} - \lambda_{e+1}\frac{T_E-T_P}{\xi_{PE}^{\,2}}\right) + Q\Delta V \quad (4.32\text{ b})$$

where $Y_{i,E+1}$ and T_{E+1} are the molar fraction of gaseous species and particle temperature of the node to the east from $Y_{i,E}$ and T_E respectively; and $\xi_{P(E+1)}$ is the distance between the node to the east from *E* and the node *E*.

Step 3. Implementation in computing program (Matlab)

I) Ordinary differential equation solver

To solve the model, equations (4.28) (4.29), as well as (i) boundary conditions in *r=0,* shown in equations (4.32 a) and (4.32 b), (ii) outer surface condition, in r=R, given in equations (4.18) and (4.21), and (iii) the molar conservation of char equation (4.2), a Matlab first-order ordinary differential equation (ode15s) solver is chosen. An ordinary differential equation (ODE) contains one or more derivatives of a dependent variable, Y_i, T and ρ_p in this case, with respect to a single independent variable, *t* (conversion time).

In an initial value problem, the ODE is solved by starting from an initial state. Using the initial condition, y_0, as well as a period of time over which the answer is to be obtained, (t_0,t_f), the solution is obtained iteratively [78]. Initial condition in this problem consists in a matrix defined as:

$$y_0 = \begin{bmatrix} \rho_{c,0,1} & Y_{O_{2,0}1} & Y_{CO_0,1} & Y_{H_{2,0},1} & Y_{CO_{2,0}1} & Y_{H_2O_0,1} & Y_{N_{2,0}1} & T_{0,1} \\ \rho_{c,0,2} & Y_{O_{2,0}2} & Y_{CO_0,2} & Y_{H_{2,0},2} & Y_{CO_{2,0}2} & Y_{H_2O_0,2} & Y_{N_{2,0}1} & T_{0,2} \\ & & & & \cdot & & & \\ & & & & \cdot & & & \\ & & & & \cdot & & & \\ \rho_{c,0,N} & Y_{O_{2,0}N} & Y_{CO_0,N} & Y_{H_{2,0},N} & Y_{CO_{2,0}N} & Y_{H_2O_0,N} & Y_{N_{2,0}N} & T_{0,N} \end{bmatrix} \quad (4.34)$$

Due to the ODE solver needs a vector as initial condition, this matrix is reformulated as a vector using the *Reshape* Matlab array, with a vector length of $N_{parameters}$ x N_{nodes}, were $N_{parameters}$ is the numbers of the parameters evaluated (molar density of char, molar fraction of the six species involved and particle temperature) and N_{node} is the total number of nodes. In the present work fifty nodes was chosen in the simulation and, as mentioned above, eight parameters are evaluated.

At each step the solver applies a particular algorithm to the results of previous steps. At the first such step, the initial condition provides the necessary information that allows the integration to proceed. The final result is that the ODE solver returns a vector of time steps $t=[t_0,t_1,t_2,...,t_f]$ as well as the corresponding solution at each step $y=[Y_0, Y_1, Y_2,..., Y_f]$ [78].

The type of ODE solver has to be chosen depending of the problem under study. Matlab provides a general guideline on when to use each of the different solvers [78]. The described ODE problem in this work is considered a stiff problem, due to the difference of the time scales (i.e. the step size taken by the solver is forced to be extremely small compared with the interval of integration). For these cases, Matlab suggest the stiff solvers (Ode15s, Ode23s, Ode23t and Ode23tb), therefore, Ode15s is selected.

II) Time dependent boundary condition at the particle surface

Since the particle shrinks as reaction proceeds, the boundary condition at the particle surface is time dependent. Beginning from $r = R$, the boundary moves towards the particles center until each cell is "fully converted" (i.e. local conversion reaches 98%). Figure 4.3 shows a scene of this phenomenon.

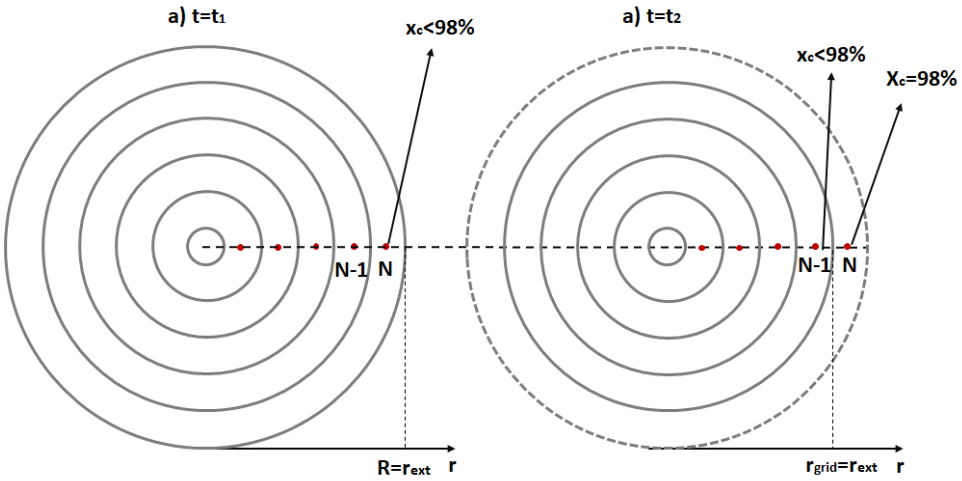

Figure 4.3 Time dependent external boundary conditions scene: a) initial particle size, b) particle size when the local conversion (x_c) of the three outer nodes have reached 98%. r_{ext} is the external particle radius.

Figure 4.4 a) represents the particle size when the local conversion in the last node (N) is below 98%. According to this model, when the local conversion reaches its maximum value (98%), the reactions in this node are nulls, in consequence, the molar density of char is constant as well as the rest of the parameters (Y_i, T) that take values corresponding to the external gas conditions. Now, the last node (N-1) and the rest of the nodes continues the simulation and the boundary conditions are updated. The correlations (Sc, Sh, Pr and Nu) and the mass and heat transfer coefficient are calculated considering the new particle size. The simulation applies this process to each control volume, until local conversion in the first node reaches 98%.

1.4 Model parameters

Table 4.1 shows the experimental data used in the model. These parameters have been obtained from direct measurements in laboratory during previous works or from the literature. In the latest case, the corresponding reference is pointed out. The model receives as input data the O_2, H_2O, CO_2 and N_2 volume fraction at the

bulk conditions and returns the molar density of the char, the volume fraction of all the gaseous species involved and the particle temperature from its surface to its center durning the conversion time. The particle diameter and bed temperature are changed in the simulation in order to know the effect of such variation on the combustion characteristics (fuel particle temperature and conversion). Likewise, Table 4.2 and 4.3 shows the kinetics parameters and the correlations applied in the model, respectively.

Table 4.1. Model parameters

Name	Value	Units	Application	Reference
d_p	0.005-0.01	m	Fuel	Measured in laboratory
d_b	0.0004	m	Bed material	Measured in laboratory
$\rho_{p.0}$	37.5	kmol/m^3	Wood-char	Measured in laboratory
ρ_b	2650	kg/m^3	Bed material	Measured in laboratory
T_b	1073-1173	K		-
$\varepsilon_{p.0}$	0,5	-	coal-char	[73]
ε_p	$\varepsilon_{p.0}$+(1- $\varepsilon_{p.0}$) x_c	-	coal-char	[74]
s_0	1 10^8		coal char	[73]
λ_p	0.08 – 0.0001 (T – 273)	(W/m·K)	Wood-char	[69]
C_p	1.003 + 2.09 (T – 273)	(kJ/kg·K)	Wood-char	[69]
e_p	0.8	-	Wood-char	[70]
e_b	0.65	-	SiO_2	[71,72]
ε_{mf}	0.4	-	SiO_2	[40]
τ_b	1.22	-	Fluidized bed	[76]
u_{mf}	0.18	m/s	Bed material	Measured in laboratory (Appendix II)
u_f	2 u_{mf}	m/s		Measured in laboratory

Table 4.2 ***Kinetic parameters***

Name	Value	Units	Applications	References
$A_{CO/CO2}$	2512	-	coal-char	[61]
$E_{CO/CO2}$	51880	J/mol	coal-char	[61]
A_{O_2}	25,42	kmol/(m^{2}s)	coal-char	[73]
E_{O_2}	179400	J/mol	coal-char	[73]
A_{CO_2}	589	m/(sK)	coal-char	[79]
E_{CO_2}	222815.2	J/mol	coal-char	[79]
E_{H_2O}	589	m/(sK)	coal-char	[79]
E_{H_2O}	222815.2	J/mol	coal-char	[79]
s_0	$1{\cdot}10^8$	m^2/m^3	coal-char	[73]

Table 4.3 Correlations

Name	Expression	Reference
Nu	$(7\text{-}10\varepsilon_b + 5{\varepsilon_b}^2)\left(1 + 0.7\,Re^{0.2}Pr^{\frac{1}{3}}\right) + (1.33 - 2.4\varepsilon_b + 1.2{\varepsilon_b}^2)Re^{0.7}Pr^{1/3}$	[64]
Sh	$2\,\varepsilon_{mf} + 0.7(Re_{mf}/\varepsilon_{mf})^{1/2}\,{Sc_i}^{1/3}$	[62]
Cd	$\left(0.63 + \frac{4.8}{Re^{0.5}}\right)^2$	[63]

Chapter 5.
Resuls and discussion

In this work, experimental and theoretical results of the maximum particle temperature in oxy-fuel combustion conditions have been studied. The theoretical model is validated with the experimental results of combustion test in O_2/N_2 and O_2/CO_2 atmosphere, and it is applied to predict the cases with steam atmosphere. In this chapter the experimental and theoretical results are shown and discussed.

1. The influence of the CO_2 gas concentration on the char temperature and conversion during oxy-fuel combustion in a fluidized bed at high O_2 concentration

In this section, results from oxy-fuel combustion tests of single char particles in a fluidized bed are shown. As described in Chapter 3, the bed temperature was 800 ºC and the O_2 concentrations were 40, 50, 60 and 70 $\%_{v/v}$, respectively, being the rest N_2 (in O_2/ N_2 tests) or CO_2 (in O_2/ CO_2 tests). Some of the published measurements by the author in ref. [26] with an O_2 concentration of 11, 21 and 30 $\%_{v/v}$, are also used here to complete the work. The analysis of temperature and apparent conversion was done according to Appendix I.

Figure 5.1 shows the apparent conversion rate: r_c (see Appendix I), and the maximum surface temperature: $T_{c,max}$, of one char particles during its conversion process under oxy-fuel combustion (O_2/CO_2) and combustion (O_2/N_2) conditions in an FB at 800 ºC. The almost linear increase in both apparent conversion rate and the maximum temperature with the O_2 concentration agree well with recent results at O_2 concentrations up to 40 $\%_{v/v}$ in O_2/CO_2 and O_2/N_2 mixtures [26]. The results in Figure 5.1 confirm that the resistance to mass transport in the gas-boundary layer controls the overall rate of conversion, as it has been pointed in refs [25, 26, 80], where the tests were carried out with mixtures of O_2/N_2.

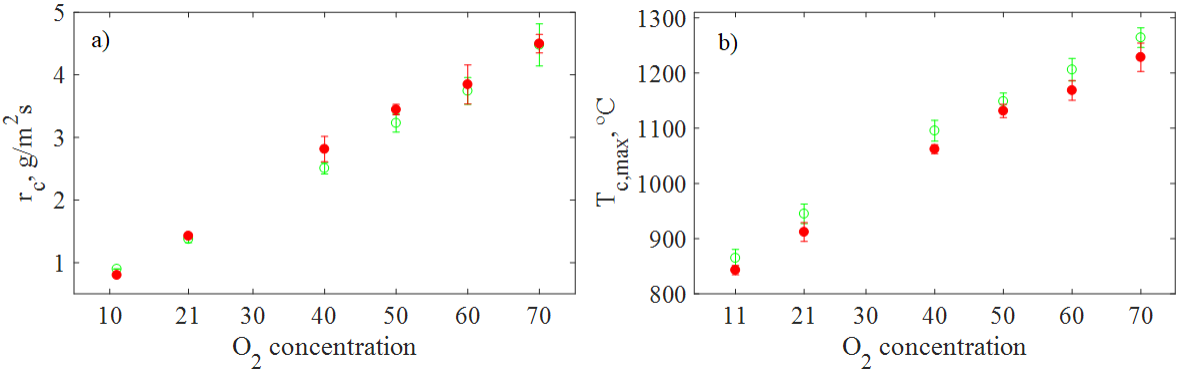

Figure 5.1 Effect of the fluidization flow, O_2/N_2 (filled symbol) vs. O_2/CO_2 (empty symbol), on the apparent consumption rate: r_c by Eq. 1 (a) and on the maximum temperature: $T_{c,max}$ (b) of char particles from

The maximum temperature measured under O_2/CO_2 environment was always lower than that measured in O_2/N_2 for a same O_2 concentration. This is in line with the lower diffusivity of O_2 through CO_2 as compared to that through N_2 (about 20 % lower [26]), which would lead to a lower conversion rate of the exothermic oxidation reaction. Surprisingly, for O_2 concentrations above 21%, the measured apparent conversion is

higher with CO_2 and with N_2, which indicates the contribution of an additional conversion reaction besides the oxidation by O_2. It is suggested that the gasification reaction (endothermic) is superimposed to the oxidation by O_2 (exothermic), which seems to be noticeable at particle temperatures above 900ºC. However, form O_2 concentration of 60 %v/v, the apparent consumption rates in O_2/CO_2 is quite similar than that in the equivalent O_2/N_2. The lower CO_2 concentration can explain the similar result in both atmosphere (lower influence of gasification).

The contribution of the gasification reaction to the overall carbon conversion has been pointed out by several authors. Scala et al. [81] studied the oxy-combustion of single bituminous char particles in an FB at 800, 850, and 900 ºC with an O_2 concentration of 2 $\%_{v/v}$, and showed that the share of the gasification reaction to the overall conversion rate was in the range of 10 and 40 % when the char temperature was about 850 and 900 ºC. Roy et al. [32] studied the oxy-fuel combustion of a single coarse char particles from Victorian brown coal in a FB at 890 ºC fluidized with an O_2 concentration from 5 to 15 $\%_{v/v}$, and showed similar contributions to those by Scala et al. In a theoretical analysis by Bu et al. [45] the contribution of gasification reached 15 % for a 6 mm lignite char particle at bed temperature of 950 ºC and with an O_2 concentration of 5 $\%_{v/v}$.

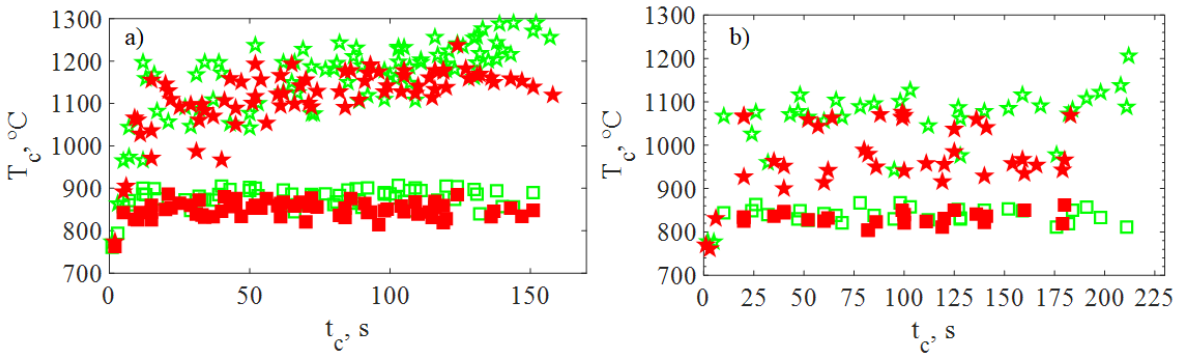

Figure 5.2 Measured surface temperature of a char particle from beech wood (8mm) in a fluidized bed at 800 ºC with an O_2 concentration of 40 and 60 %v/v in N_2 (empty symbols) and in CO_2 (filled symbols). Star symbol: particle temperature in the emulsion phase. Square symbol: particle temperature in the splash zone and the bubble phase.

Figure 5.2 shows the surface temperatures of the char particle when the particle is located in the emulsion phase (square symbol) and splash-zone or bubble phase (star symbol). The measurements are for 40 and 60 $\%_{v/v}$ O_2 concentration both in N_2 and in CO_2. In the figure, the temperature of the char particle is lower and more stable when the particle is in the emulsion phase than in the splash zone or the bubble phase. This can be explained by the quenching effect of the bed on the char particle that keeps the particle temperature close to that of the bed. In contrast, in the bubble phase and the splash zone the temperature is higher due to the higher gas velocity surrounding the char particle and the consequently higher oxidation rate. The wider range of temperatures measured in the splash zone and bubble phase (temperature differences of hundreds of degrees) compared to the range measured in the emulsion phase, reflects that the camera has captured the particle at different points during its heat up process from the temperature in the emulsion phase to the maximum temperature reached when it is out of the bed. Further, the differences between the temperatures of the char particle in the emulsion phase and out of it seem to increase with the O_2 concentration, in agreement with the observations in Ref. [80] for O_2 concentrations higher than 21 $\%_{v/v}$ in N_2.

On the other hand, in the Figure 5.3 the experimental and theoretical (predicted by the model) results of the evolution of the surface particle temperature during its conversion, of beech wood char particle are shown. Figure 5.3 a) and b) represents the results in a O_2/N_2 and O_2/CO_2 atmosphere, respectively. It seems that the predicted results are in line with the experiments. On the one hand, surface temperature in O_2/CO_2 atmosphere is lower than in O_2/N_2 atmosphere due to the lower diffusivity of O_2 in CO_2 compared with those in N_2. On the other hand, the surface temperature increases as the combustion proceeds showing the maximum temperatures at the end of the conversion.

The maximum and minimum particle temperature recorded experimentally during the fuel combustion shows differences of hundreds degrees as it is discussed above. The predicted results shows temperature values

inside the range of temperature in each atmosphere.

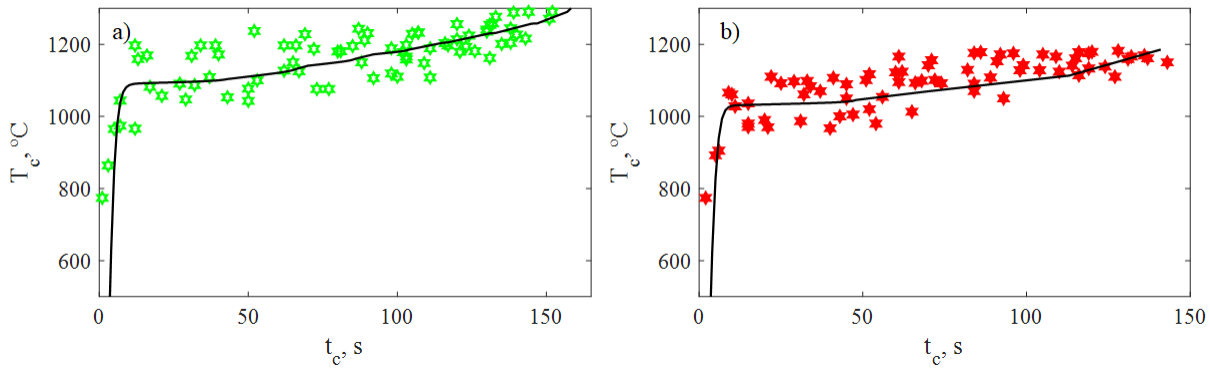

Figure 5.3 Predicted (solid line) and measured (symbol) evolution of a surface beech wood particle temperature (8 mm) during its conversion, in a fluidized bed at 800 °C with an O_2 concentration of 60 %v/v in N_2 (empty symbols) and in CO_2 (filled symbols)

Figure 5.4 shows the experimental (symbol) and predicted (solid line) burnout time by the theoretical model. It is visible that the predicted values agrees with the experimental results, giving an error below 15% both in N_2 (a) and CO_2 (b) atmosphere. In Figure 5.4 a) the solid and dotted lines indicate the predictions by the model accunting with and without the gasification reaction, respectively. This result shows that the influence of gasification reaction increases with the O_2 concentration, being negligible at O_2 concentration of 21%. Therefore, it is clear that the gasification reaction is necessary to explain the experimental results at high O_2 concentration, which confirms the hypothesis formulated above.

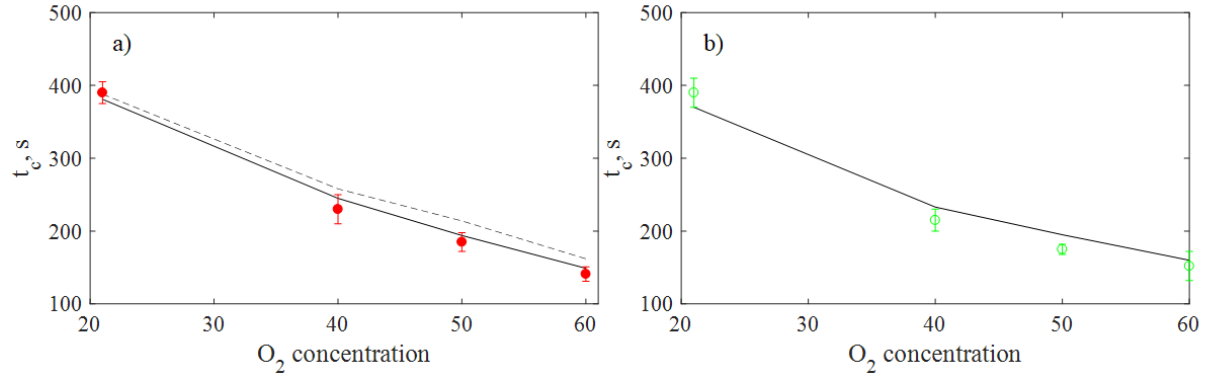

Figure 5.4 Experimental and predicted burnout time of a char particle from beech wood in a fluidized bed at 800 °C with an O_2 concentration of 21, 40, 50, 60 and 70 %v/v in a) CO_2 with (solid line) and without (dotted line) gasification reaction considered in the simulation and b) N_2. Filled symbol: experimental burnout time.

2. The predicted effect of steam concentration in oxy-fuel combustion

Figure 5.5 shows the peak particle temperature and burnout time predicted by the theoretical model in oxy-fuel conditions with 10-21-40-50-60% O_2 in N_2, CO_2 and water vapor, respectively. Compared to a similar case with CO_2, in an atmosphere with water vapor the conversion time is shorter and the peak particle temperature is higher. This is in good agreement with the results of Marek et al. [31] with mm-sized char particles and a horizontal furnace, and with the results by Roy et al [32] in a fluidized bed.

The higher diffusivity of O_2 in H_2O than that of O_2 in CO_2 allows that a higher amount of O_2 reaches to the particle surface, therefore, high amout of O_2 reacts with the fuel, and that produce a higher particle temperature and a higher conversion rate. This phenomenon is shown in Figure 5.6 a) and c). This figure represents the O_2 concentration profile in each case (i.e O_2/CO_2, and O_2/H_2O atmosphere) for a beech wood char particle after 200 second of reaction at O_2 concentration of 21%. It is visible that the O_2 concentration in the particle surface is higher in O_2/H_2O than in O_2/CO_2 atmosphere leading to a high conversion rate. In fact, at the same conversion time the particle size (R) in oxy-steam case is lower than in oxy-CO_2 case (3.5 mm vs. 4 mm).

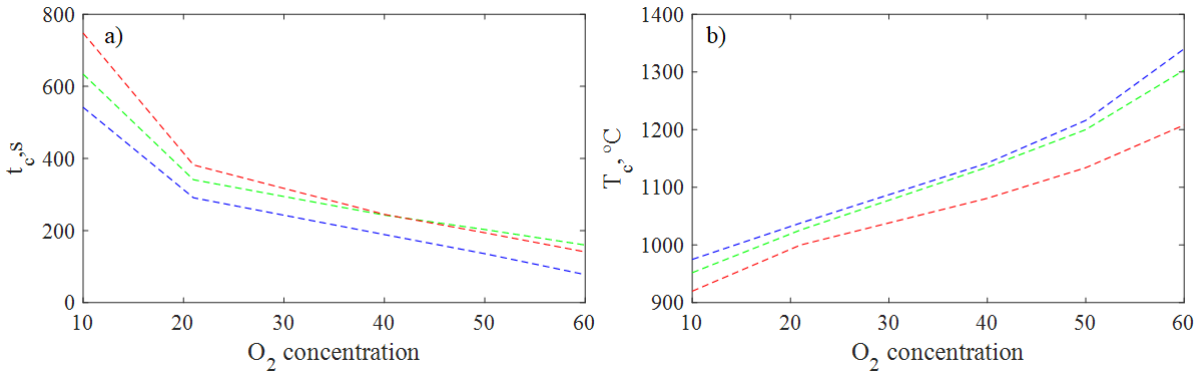

Figure 5.5. Predicted burnout time and maximum temperature of a char particle from beech wood in a fluidized bed at 800 ºC with an O_2 concentration from 10 to 60 %v/v in N_2 (green) CO_2 (red) and H_2O (blue). Symbol: experimental data. Solid line: Predicted data

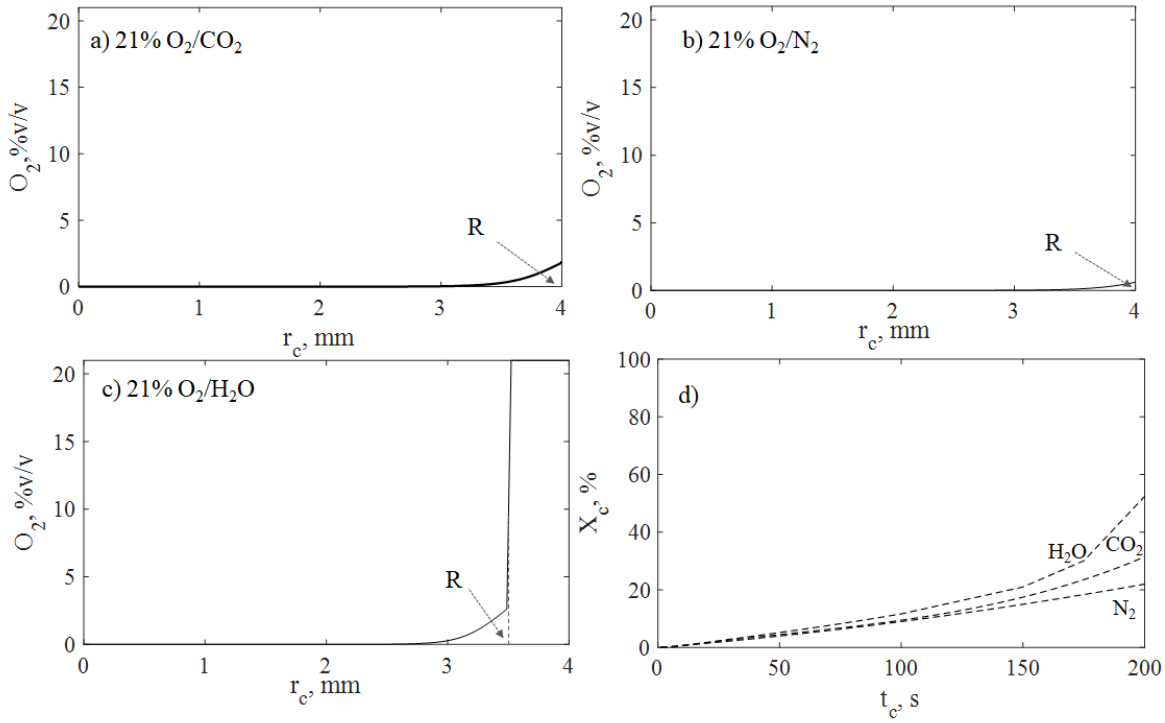

Figure 5.6 Concentration profile of O_2 in a) oxy-CO_2 and b) oxy-steam process for a beech wood char particle at 200 second of reaction.

Figure 5.6 b) shows the O_2 concentration profile in O_2/N_2 atmosphere and Figure 5.6 c) represents the overall conversion rate in each case. It is observable that the O_2 concentration in the particle surface is also higher in O_2/H_2O than in O_2/N_2 atmosphere, due to the same reason discussed above for CO_2 case (i.e. the difussivity of O_2 in water vapor is higher than that in N_2). Therefore, a higher peak temperature and conversion rate in oxy-steam case is expected. However, the particle temperature in O_2/H_2O and O_2/N_2 are quite similar for concentrations above 21%. This result indicate that the gasification reaction contributes in this process by decreassing the particle temperature (Figure 5.5 b).

According to these results, it is expected that in oxy-fuel combustion with wet recirculation the maximum particle temperature would be higher than in a similar case with dry recirculation. This is the result of increasing the apparent diffusivity of the gas when adding a share of water vapor. This is shown in Fig 5.7 a), according to the model predictions. The burnout time decreases as the concentration of steam increases, while the maximum particle temperature increases (Fig 5.7 b)). This relationship (steam concentration vs. particle

temperature) was observed experimentally by Marek et al. [31] in an investigation with cubic-shape char particles in different oxy-fuel atmospheres. Figure 5.8 shows the results from studies of Marek et al. and from simulations carried out in this work.

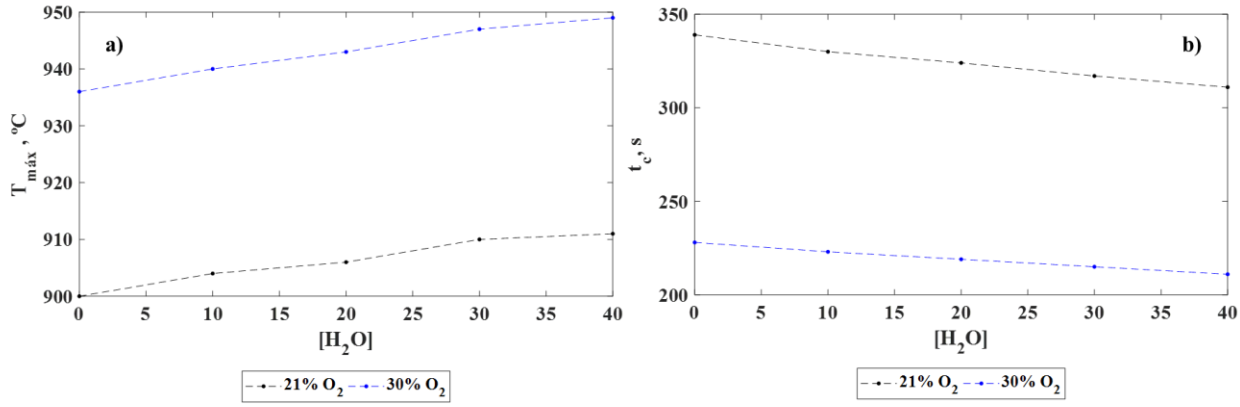

Figure 5.7. Predicted maximum temperature and burnout time of a char particle from beech wood in a fluidized bed at 800 ºC with an O_2 concentration of 21 and 30 %v/v in CO_2/H_2O atmosphere at H_2O concentration from 0 to 40%v/v.

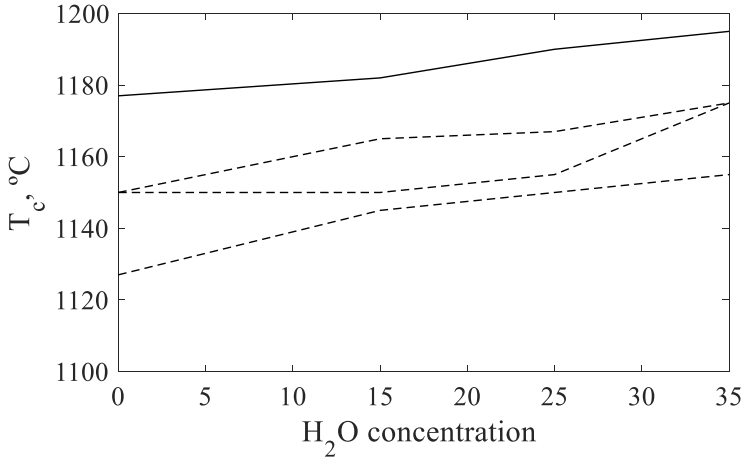

Figure 5.8. Experimental average temperature of several types of carbon and char during its combustion at steam concentrations from 0 to 35%v/v in $O_2/CO_2/H_2O$ atmosphere. Dotted lines: Particle temperature measured by Marek et al. in two types of bituminous char [31]. Solid line: Particle temperature predicted by the model for a bituminous char.

Chapter 6.
Conclusions and further work

In this work, the influence of CO_2 and water vapor on the particle temperature and conversion of the beech wood char has been studied experimentally and theoretically by a one-dimensional model. The effect of CO_2 has been studied by measuring the particle temperature and burnout time in a lab-scale fluidized bed reactor. This study covers experimental results from 21% to 70% O_2 concentration in both N_2 and CO_2.The experimental measurements of the particle temperature have been carried out by pyrometry using a digital camera. Before the experiments, this measurement methodology required a calibration process of the camera that also has been carried out in this work.

The predicted results agree well with the experiments giving an error in burnout time below 15% both in N_2 and CO_2 atmosphere, and showing an evolution of the particle temperature with the time inside the range of the particle temperatures measured in each case (i.e. O_2N_2/O_2CO_2 atmosphere). The conclusions from these experiments and simulations are the follow:

i) The surface particle temperature reached by the particle during its combustion increase as the O_2 concentration increase, due to the strongly influence of O_2 diffusion through the bulk gases to the particle surface.

ii) The surface particle in O_2/CO_2 atmosphere is lower than in O_2/N_2 atmosphere due to the lower diffusivity of O_2 in CO_2 than that in N_2.

iii) The conversion rate in O_2/CO_2 atmosphere is higher than in O_2/N_2 when the particle temperature is obove 900ºC due to the contribution of the gasification reaction.

iv) At O_2 concentration higher than 50% the conversion rate in O_2/CO_2 and in O_2/N_2 is quite similar. This could be explained by the lower contribution of gasification reaction at these conditions due to the lower presence of CO_2.

The influence of H_2O in oxy-fuel combustion has been studied by the theoretical model developed, taking into account the physico-chemical properties of H_2O in the simulations. Predicted results shows that:

i) The particle temperature in O_2-steam is higher than that obtained in O_2/CO_2. Therefore, the particle temperature when the steam is added to an O_2/CO_2 mixture (i.e. the apparent diffusivity of the gas is higher when adding a share of water vapor).

ii) The conversion rate is higher in water vapor than in the other cases due to two phenomena: O_2 diffusivity in steam is higher than in N_2 and CO_2 and the contribution of the gasification reaction.

iii) When O_2 concentration is higher than 21% the particle temperature in O_2/H_2O and O_2/N_2 is quite similar. This is due to the contribution of the endothermic gasification reaction.

However, in this work, the predictions related to oxyfuel combustion in the presence of steam have been exclusively theoretical. Further work is needed to validate the model with experimental results.

Nomenclature

Notations

$A_{CO/CO2}$	pre-exponential factor, –
A	pre-exponential factor for kinetic reaction of char, kmol/(m^2 s)
C_p	specific heat at constant pressure, kJ/(kg K)
$E_{CO/CO2}$	activation energy, kJ/mol
E	activation energy for kinetic reaction of char, kJ/mol
e_{eff}	effective emissivity of the radiative exchange between bed and char particle
D	molecular diffusivity, m^2/s
h_{conv}	heat transfer coefficient, W/(m^2 K)
h_m	mass transfer coefficient, m/s
k	kinetic reactivity of heterogeneous reaction, kg/(m^2 s)
M	molecular mass, mol/kg
Nu	Nusselt number
Pr	Prandtl number
r	distance from the particle's center, m
R	initial radius of fuel particle, m
R_g	gas constant
R_v	reaction rate, kg/(m^3 s)
s	specific surface area, m^2/m^3
S	source mass term, kg/(m^3 s)
Q	source heat term, W
Sh	Sherwood number
t	time, s
T	temperature, K
u	gas velocity, m/s
x	carbon conversion of the particle

Nomenclature

Y	mass fraction
FGC	Flue gases conditioner
ESP	Electrostatic precipitator
FB	Fluidized bed
CCS	CO_2 compression, capture and storage
SMOC	steam-moderated oxy-fuel combustion
ER	Entrained reactor
TGA	Thermogravimetric Analyzer
DTF	Drop tube furnace
CFD	Computational fluid dynamic
Greek letters	
ε	porosity, or bed voidage
λ	thermal conductivity, W/(m K)
ΔH	heat of chemical reaction, J/kg
ρ	density, kg/m3
σ	Stephan–Boltzmann constant
Subscripts	
b	bed materials
conv	convection
eff	effective
g	gas
i, j	components
m	mass
p	char particle
s	particle surface
0	initial value
∞	under bulk conditions

References

[1] https://www.theguardian.com/environment/2011/feb/04/man-made-greenhouse-gases ida.

[2] http://climate.org/humansandthegreenhouseffect

[3] http://css.snre.umich.edu/factsheets/climate-change-science-and-impacts-factsheet

[4]http://www.environment.gov.au/climate-change/climate-science-data/climate-science/greenhouse-effect

[5] https://www.theguardian.com/environment/2011/feb/04/man-made-greenhouse-gases.

[6] BP Energy Outlook 2019- BP Global, 2019 Edition

[7] Alfons Kather, Sven Kownatzki, Assessment of the different parameters affecting the CO_2 purity from coal fired oxyfuel process, International Journal of Greenhouse Gas Control, 2011

[8] B.J.P. Buhre, L.K. Elliott, C.D. Sheng, R.P. Gupta, T.F. Wall, Oxy-fuel combustion technology for coal-fired power generation, Progress in Energy and Combustion Science 31;283–307, 2005

[9] Liyong Wang, Experimental and modeling study of SO_2 behavior during oxy combustion in fluidized beds, 2012

[10] Günter Scheffknecht∗, Leema Al-Makhadmeh1, Uwe Schnell, Jörg Maier, Oxy-fuel coal combustion, A review of the current state-of-the-art, International Journal of Greenhouse Gas Control, 2011

[11] Terry Wall, Yinghui Liua, Chris Spero, Liza Elliot, Sameer Kharea, Renu Rathnama, Farida Zeenathala, Behdad Moghtaderia, Bart Buhred, Changdong Shenge, Raj Guptaf, Toshihiko Yamadac, Keiji Makinoc, Jianglong Yua,g. An overview on oxyfuel coal combustion—State of the art research and technology development,, chemical engineering research and design 87; 1003–1016, 2009

[12] B.J.P. Buhre, L.K. Elliott, C.D. Sheng, R.P. Gupta, T.F. Wall, Oxy-fuel combustion technology for coal-fired power generation, Progress in energy and combustion science, 31 (2005) 283–307

[13] Riaza J. Khatami R, Levendis YA, Álvarez L, Gil MV, Pevida C, Rubiera F, Pis JJ, Single particle ignition and combustion of anthracite, semi-anthracite and bituminous coals in air and simulated oxy-fuel conditions. Combustion and Flame 2014; 161; 1096-1108

[14] Singer S,Chen L, Ghoniem AF. The influence of gasification reactions on char consumption under oxy-combustion conditions: Effects of particles trajectory and conversion. Proceedings of the Combustion Institute 2013; 34; 3471-3478

[15] Marek E, Swiatkowski B. Experimental studies of single particle combustion in air and different oxy-fuel atmospheres. Applied Thermal Engineering 2014; 66; 35-42

[16] Hecht ES, Shaddix CR, Molina A, Haynes BS, Effect of CO_2 gasification reaction on oxy-combustion of pulverized coal char. Proceeding of the Combustion Institute 2011; 33; 1699-1706

[17] Gonzalo-Tirado C, Jiménez S, Ballester J. Gasification of a pulverized sub-bituminous coal in CO2 at

atmospheric pressure in an entrained flow reactor. Combustion and Flame 2012; 15; 385-395

[18] Kim D, Choi S, Shaddix CR, Geier M, Effect of CO_2 gasification reaction of char particles combustion in oxy-fuel conditions Fuel 2014; 120; 130-140

[19] Leckner Bo, Gómez-Barea A. Oxy-fuel combustion in circulating fluidized bed boilers, Applied Energy 2014; 125; 308-318

[20] Günther C, Weng M, Kather A. Restrictions and limitation for the design of a steam generator for a coal-fired oxyfuel power plant with circulating fluidized bed combustion. Energy Procedia 2013; 34; 3471-3478

[21] Scala F, Chirone R, Fluidized bed combustion of single coal char particles at high CO_2 concentration, Chemical Engineering Journal 165 (2010) p. 902-906

[22] Wanga W, Changsheng Bu C, Gómez–Barea A, Leckner B, Wanga X, Zhanga J, Piao G, O_2/CO_2 and O_2/N_2 combustion of bituminous char particles in a bubbling fluidized bed under simulated combustor conditions, Chemical Engineering Journal 336 (2018) 74–81

[23] Bu C, Liu D, Chen X, Pallarès D, Gómez-Barea A, Ignition behavior of single coal particle in a fluidized bed under O_2/CO_2 and O_2/N_2 atmospheres: A combination of visual image and particle temperature, Apply Energy 115 (2014) p. 301-308

[24] Bu C, Leckner B, Chen X, Pallarès D, Liu D, Gómez-Barea A, Devolatilization of a single fuel particle in a fluidized bed under oxy-combustion conditions. Part A: Experimental results, Combustion and Flame 162 (2015) p. 797-808

[25] Bu C, Pallarès D, Chen X, Gómez-Barea A, Liu D, Leckner B, Lu P, Oxy-fuel combustion of a single fuel particle in a fluidized bed: Char combustion characteristics, an experimental study, Chemical Engineering Journal 287 (2016) p. 649-656

[26] Salinero J, Gómez-Barea A, Fuentes-Canoa D, Leckner B, The influence of CO_2 gas concentration on the char temperature and conversion during oxy-fuel combustion in a fluidized bed, Applied Energy 215 (2018) 116–130

[27] Lei Cai, Chun Zou, Yanwen Guan, Huiqiao Jia, Lian Zhang, Chuguang Zheng, Effect of steam on ignition of pulverized coal particles in oxy-fuel combustion in a drop tube furnace, Fuel; 958-966, 2016

[28] Riaza J. Álvarez L., Pevida C, Pis JJ, Rubiera F. Effect of oxy-fuel combustion with steam addition on coal ignition and burnout in a entreined flow reactor. Energy 2011; 36:5314-9

[29] Gil MV, Riaza J., Alvarez L., Pevida C, Pis JJ, Rubiera F, A study of oxycoal combustion with steam addition on coal ignition and biomass blending by thermogravimetric analysis. J Therm Anal Calorim 2012;109:49-55

[30] Baojun Yi, Liqi Zhang, Fang Huang, Zhihui Mao, Chuguang Zheng, Effect of H_2O on the combustion characteristics of pulverized coal in O_2/CO_2 atmosphere, Applied Energy 132; 349–357, 2014

[31] Ewa Marek, Bartosz Swiatkowsi, Experimental studies of single particle combustion in air different oxy-fuel atmospheres, Applied Thermal Engineering, Volume 74, Pages 61-68, 2015

[32] Bithi Roy, Sanka Bhattacharya, Combustion of single char particles from Victorian Brown coal under oxy-fuel fluidized bed conditions, Fuel 165; 477-483, 2016

[33] Chun Zou, Liang Zhang, Shiying Cao, Chuguang Zheng, A study of combustion characteristics of pulverized coal in O_2/H_2O atmosphere, Fuel 115; 312-320, 2014

[34] Chung Zou, Lei Cai, Di Wu, Yang Liu, Siliang Liu, Chuguang Zheng, Ignition behaviors of pulverized coal particles in O_2/N_2 and O_2/H_2O mixtures in a drop tube furnance using flame monitoring techniques, Proceedings of the Combustion Institute 35; 3629-3636, 2015

[35] Lei Cai, Chun Zou, Yang Liu, Kai Zhou, Qingsong Han, Chuguang Zheng, Numerical and experimental studies on the ignition of pulverized coal in O_2/H_2O atmospheres, Fuel 139; 198-205, 2015

[36] Liang Zhang, Chung Zou, Di Wu, Yang Liu, Chuguang Zheng, A study of coal char combustion in O_2/H_2O, J. Therm. Anal. Calorim.; 126:995-1005, 2016

[37] Kai Lei, Buqing Ye, Jin Cao, Rui Zhang and Dong Liu, Combustion characteristics of single particles from bituminous coal and pine sawdust in O_2/N_2, O_2/CO_2, and O_2/H_2O Atmospheres, Energies 10, 2017

[38] Toftegaard MB, Oxy-fuel combustion of coal and biomass. DTU Chemical Engineering, 2011 (Ph.D Thesis)

[39] S. Nakayama and Y. Noguchi, Pulverized Coal Combustion in O_2/CO_2 Mixtures on a Power Plant for CO_2 Recovery, Energy Convers. Mgmt 33, No. 5-8; 379-386, 1992

[40] Obras-Loscertales M de las, Rufas A, de Diego LF, García-Labiano F, Gayán P, Abad A, Adánez J. Effects of temperature and flue gas recycle on the SO_2 and NOx emissions in an oxy-fuel fluidized bed combustor. Energy Proc ;37:1275–82, 2013

[41] Diego LF, Obras-Loscertales M de las, Rufas A, García-Labiano F, Gayán P, Abad A, Adánez J. Pollutant emissions in a bubbling fluidized bed combustor working in oxy-fuel operating conditions: Effect of flue gas recirculation, Applied Energy 102; 860–867, 2013

[42] Salvador C, Mitrovic M, Zanganeh K. Novel oxy-steam burner for zero-emission power plants (power point presentation). Canmet Energy; 2009

[43] Sivaji Seepana, Sreenivas Jayanti, Steam-moderated oxy-fuel combustion, Energy Conversion and Management 51; 1981–1988, 2010

[44] A. Macek, C. Bulik«Direct Measurement of Char Particle Temperatures in Fluidized Bed Combustors, The Combustion Institute, pp. 1223-1230, 1984

[45] Bu, C, Gómez-Barea A, Chen X, Leckner B, D. Liu D, Pallarès D, Lu P, Effect of CO_2 on oxy-fuel combustion of coal-char particles in a fluidized bed: Modeling and comparison with the conventional mode of combustion, Applied Energy 177 (2016) p. 247-259

[46] Salinero J, Gómez-Barea A, Fuentes-Cano D, Leckner B. The effect of using thermocouples on the char particle combustion in a fluidized bed reactor. Fuel 207 (2017) p. 615-624

[47] Salinero J, Gómez-Barea A, Fuentes-Cano D, Leahy JJ, Leckner B. Impact of using thermocouples to measure char particle temperature in a fluidized bed combustor. 12nd International Conference on Fluidized Bed Technology 1 (2017) p. 655-662

[48] A. Macek, C. Bulik, Direct Measurement of Char Particle Temperatures in Fluidized Bed Combustors, The Combustion Institute, pp. 1223-1230, 1984

[49] Salinero J, Measurement of char temperature in a fluidized bed reactor using pyrometry with a digital camera: application to oxy-fuel combustion, Doctoral thesis, University of Seville, 2018

[50] Salinero J, Measurement of the surface temperature of char in combustion in a fluidized bed by pyrometry with digital camera, Master thesis, University of Seville, 2015.

[51] Salinero J, Gómez-Barea A, Leckner B, Tripiana M, Bu B, Gómez-González E. Improving char temperature measurement by pyrometry with digital camera. Proceedings of 22nd International Conference

on Fluidized Bed Conversion Turku (Finland), 2 (2015) 375-383

[52] Lu H, Leong-Teng I, Mackrory A, Werrett L, Scott J, Tree D, Baxter L. Particle surface temperature measurements with multicolor band pyrometry, AIChE Journal 2009; 55; 243– 255.

[53] Berdugo A. Medida de la temperatura superficial del carbonizado de haya en un reactor de lecho fluido mediante pirometría para aclarar el efecto del CO2 en oxi-combustión pirometría para aclarar el efecto del CO_2, TFG, University of Seville, 2016

[54] Saastamoinen J, Tourunen A, Pikkarainen T, Hasa H, Miettinen J, Hyppanen T, Myohanen K, Fluidized bed combustion in high concentrations of O2 and CO2, Proceeding of the 19th International Conference on Fluidized Bed Combustion 49 (2006)

[55] Sheng L, Liu X, Si J, Xu Y., Zhou Z., Xu M, Simulation and comparative exergy analyses of oxy-steamcombustion and O_2/CO_2 recycled combustion pulverized-coal-firedpower plants, International Journal of Greenhouse Gas Control 27 (2014) 267–278

[56] Gómez-Barea A, Leckner B, Modeling of biomass gasification in fluidized bed, Progress in Energy and Combustion Science 36 (2010) 444-509

[57] Kreitzberg T, Phounglamcheik A, Bormann C, Kneer R, and Umeki K, The change in size of char particles during combustion and gasification in regime II, June 2019

[58] Fabrizo Scala, Fluidized bed technologies for near-zero emission combustion and gasification, Chapter 7, 2013

[59] Sean C. Garrick, Michael Bühlmann, Modeling of gas to particle mass transfer in turbulent flows, Chapter 1, 2018

[60] Changsheng Bu, Alberto Gómez-Barea, Xiaoping Chen, Bo Leckner, Daoying Liu, David Pallarès, Ping Lu, Effect of CO2 on oxy-fuel combustion of coal-char particles in a fluidized bed: Modelling and comparison with the conventional mode of combustion, 2016; Applied Energy 177 (2016) 247–259

[61] Arthur JR. Reactions between carbon and oxygen. Faraday Soc Trans 1951; 47 (1):164–78.

[62] Scala F, Mass transfer around freely moving active particles in the dense phaseof a gas fluidized bed of inert particles, Chemical Engineering Science 62 (2007) 4159–4176

[63] Geng Y, Che D, An extended DEM–CFD model for char combustion in a bubbling fluidized bed combustor of inert sand, Chemical Engineering Science 66 (2011) 207–219

[64] Gunn, D.J., Transfer of heat or mass to particles in fixed and fluidized Beds. International Journal of Heat and Mass Transfer 21,467–476, 1978

[65] V.A. Borodulya V.I. Kovensky, Radiative heat transfer between a fluidized bed and a surface, Int. J. Heat Mass Transfer. Vol. 26. No. 2. pp. 277-287, 1983

[66] SK Bhatia, DD Perlmutter, A random pore model for fluid solid reaction: I. Isothermal, kinetic control, AiChE J. 26 379-386, 1980

[67] Morin M, Pécate S, Hémati M, Kinetic study of biomass char combustion in a low temperaturefluidized bedreactor, Chemical engineering journal, 331 265-277, 2018

[68] Magnaterra M, Fusco J.R, Ochoa J, Cukierman AL, Kinetic study of the reaction of different hardwood sawdust chars with oxygen. Chemical and structural characterization of the samples, Advances in

thermoquemical biomass conversion, 116-130, 1993

[69] GM Wiggins, PN Ciesielski, CS Daw , Low-Order Modeling of Internal Heat Transfer in Biomass Particle Pyrolysis, - Energy & Fuels, 30, 6, 4960-4969 2016

[70] K. W. Ragland, D. J. Aerts, Properties of Wood for Combustion Analysis, Bioresource Technology 37 161-168, 1991

[71] Yamada J, Kurosaki Y, Nagai T, Radiation Heat Transfer Between Fluidizing Particles and a Heat Transfer Surface in a Fluidized Bed, J. Heat Transfer. 123(3): 458-465, 2001

[72] Eriksson M, R. Golriz M, Radiation heat transfer in circulating fluidized bed combustors, International Journal of Thermal Sciences 44 399–409, 2005

[73] Vasilije Manovic, Mirko Komatina, Simeon Oka, Modeling the temperature in coal char particle during fluidized bed combustion, Fuel 87 (2008) 905-914

[74] Adschiri T, Kojima T, Furusawa T, Estimation of dynamic change in gasification rate of chars--ii. overlapped grain model, Chemical Engineering Science, Vol. 42, No. 6, pp. 1319-1322. 1987.

[75] D. F. Fairbanks, C. R. Wilke, Diffusion Coefficients in Multicomponent Gas Mixtures, Ind. Eng. Chem., 42, 3, 471-475, 1950

[76] Punčochář M, Drahoš J, The tortuosity concept in fixed and fluidized bed, Chemical Engineering Science. Vol. 48, No. 11. pp. 2173-2175, 1993.

[77] Versteeg H.K, Malalasekera W, An Introduction to Computational Fluid Dynamics: The Finite Volume Method, Finite volume method for 1D steady state diffusion (Chapter 4), 2007

[78] https://www.mathworks.com/help/matlab/math/choose-an-ode-solver.html

[79] Q. Xue, R.O. Fox, Multi-fluid CFD modeling of biomass gasification in polydisperse fluidized-bed gasifiers, Powder Technology, Volume 254, March 2014, Pages 187-198

[80] Salinero J, Gómez-Barea A, Fuentes-C ano D, Leckner B, Measurement and theoretical prediction of char temperature oscillation during fluidized bed combustion, Combustion and Flame, Volume 192, June 2018, Pages 190-204

[81] Scala F, Chirone. Combustion of single coal char particles under fluidized bed oxyfiring conditions, Industrial & Engineering Chemical research 49 (2010) p. 11029-11036

Appendix I
Analysis methodology

The temperature analysis methodology shall be able to detect (i) the maximum particle surface temperature in each test and (ii) the maximum temperature measurable with the technique (saturation). Because of the previous experimental results shows that most of the maximum temperatures were found in the final section of the test, the analysis of each test will apply during the second half of the total time. Therefore, after generating the images (25 fps), those belonging to this section will be selected. The following methodology shall be followed:

I. Each interval is constituted by some images (two frames at least) belonging to the same second of the test. The images where the particle is in the emulsion, splash and/or bubble zone, shall be taken in order to evaluate the temperatures leap (during the same second) produced on the char surface when the particle is in the different phases of the bed.

II. In order to obtain a pair of results (minimum and maximum temperature) every 1-2 second, the number of intervals selected will be calculated as follow:

$$Intervals = \frac{t_f}{2 \cdot nº\ tests}$$

All the intervals shall be distributed approximately uniform in order to cover all selected section of the test for the analysis.

III. After each test has been analyzed, five maximum temperatures shall be taken.

This methodology aims cover the most probability area to find the maximum char surface temperatures in order to obtain an objective result. Figure AI.1 shows the maximum and minimum char surface temperatures obtained after to apply the descripted methodology to six combustion tests at 60% O2 concentration in N2.

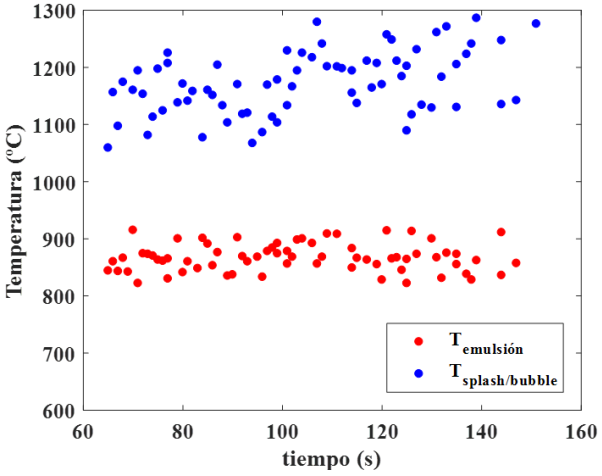

Figure AI.0.1 Maximum and minimum temperature of biomass char particle surface for the combustion tests carried out at 60% O_2 concentration in N_2.

I.AI.2 Apparent consumption rate analysis

The apparent char particle consumption rate is defined as:

$$\Gamma_c = \frac{x_{c,fx} \cdot m_{c,0}}{S_{c,0} \cdot t_{burnout}} \qquad (AI.1)$$

Where $t_{burnout}$ is the burnout time, $X_{c,fx}$ is the carbon content of the particle, $S_{c,0}$ is the external surface area in the initial time and $m_{c,0}$ is the initial mass. Each parameter is obtained as follow:

i) The initial mass of the char particle is the mass of the particle before entering in the reactor.
ii) The carbon content is estimated around 0.96% [26].
iii) The initial surface area of the particle is estimated as the surface area of a spherical particle whose diameter is calculated as:

$$d_c = \sqrt[3]{\frac{6 \cdot m_{c,0}}{\pi \cdot \rho}}$$

iv) Where ρ represents the biomass char density and it was determined experimentally in previous works [53].
v) The burnout time is defined as the last second the particle is visible, if its average diameter was below 7 pixels (~98-99% conversion). The average diameter is estimated as the average of two diameters values, as shows Figure AI.2.

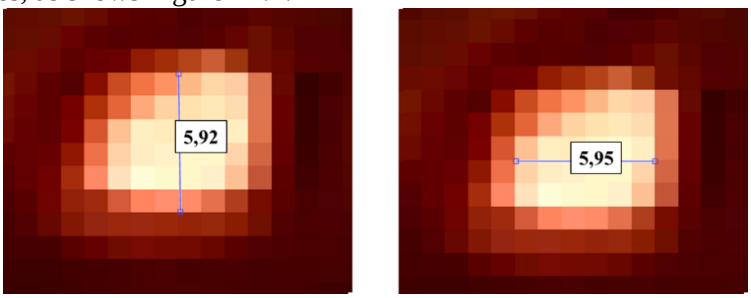

Figure AI.0.2 Last image found in a combustion test.

Appendix II
Minimum fluidization velocity

In order to determine the minimum fluidization velocity, the pressure drop in the gas distributor for different flow rates is first measured, and the curve represented in Figure AII.1a) is obtained. Then, the same procedure is performed when the reactor contains the bed material inside, the curve shown in Figure AII.1b) is obtained, which represents the addition of the pressure drop in the bed and the distributor. The bed material used is 500 g (12 cm height) of silica sand (320-500 µm). In order to ensure that the result is the same for all the experimental cases, the pressure drop curve using air, N_2 and CO_2 as inlet gas flow were measured.

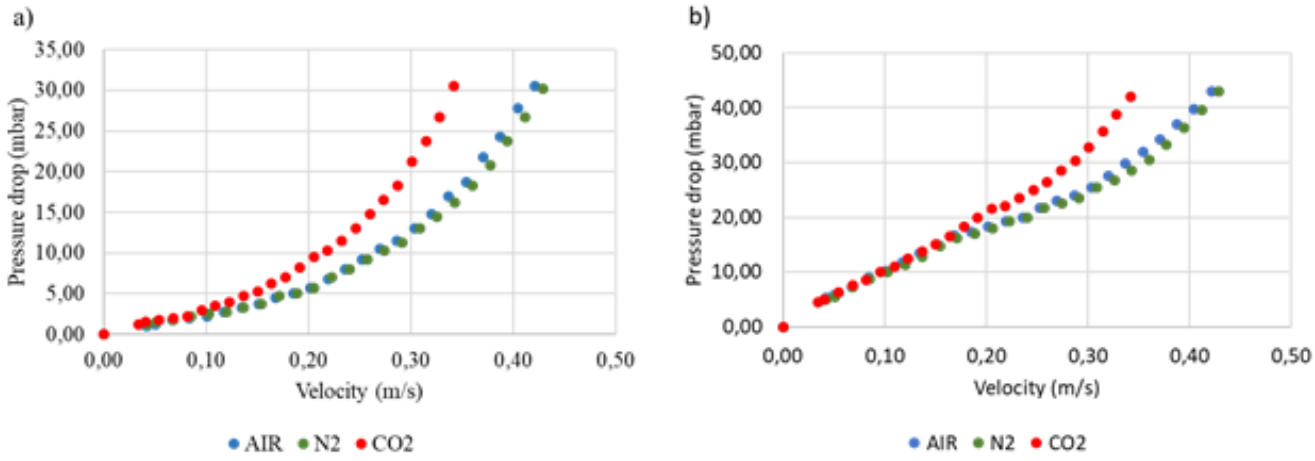

Figure AI.0.1 Pressure drop in the distributor (a) and addition of the pressure drop in the distributor plus in the material bed

The pressure drop in the bed is obtained as the difference between the two curves represented ($\Delta P_{distributor+bed}$ - $\Delta P_{distributor}$). The result is shown in Figure AII.2.

By increasing the gas velocity through the initially fixed particles of the bed material, the force applied by the gas to the bed material increases. This phenomenon causes an increase in the pressure drop of the material bed. When this force is equal to the weight of the bed, the bed particles will start a movement like a fluid (fluidization). At this moment the bed reaches the minimum fluidization velocity (U_{mf}). While the gas velocity increase (U), the pressure drop of the bed material remains constant and the bed movement becomes more turbulent (i.e. the bubble explosions occur more frequently). The minimum fluidization velocity value for the material bed used in this work is around 0.18 m/s, as shows Figure AII.2.

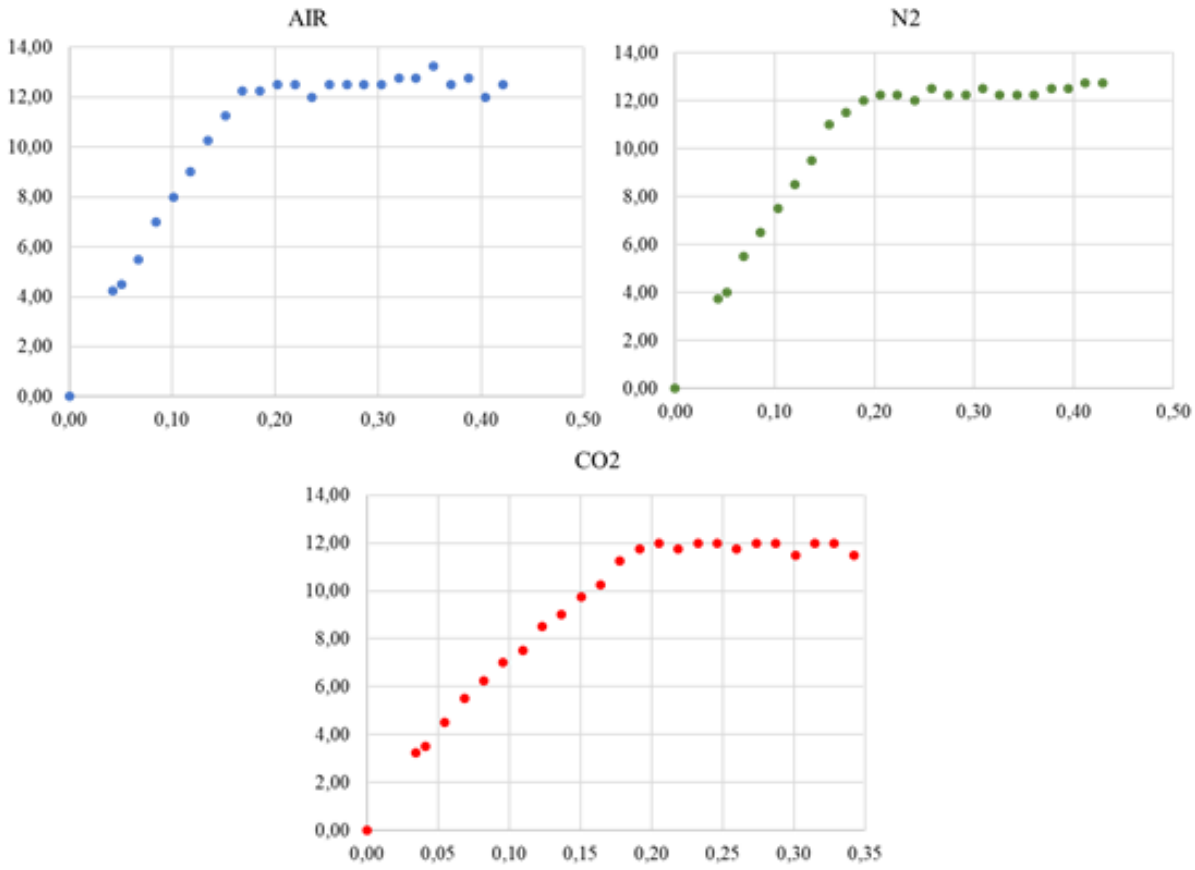

Figure AII.0.2 Pressure drop curves using air, N2 and CO2 as inlet gas flow.

Appendix III
Inlet gas concentration

In order to ensure the O_2 concentration in O_2/N_2 and O_2/CO_2 atmospheres at the inlet gas flow agree with the calculated concentration to use in the experimental tests, measurements using the micro gas-chromatograph were performed.

To carry out the O_2/N_2 calibration curve, a gas mixture of 0%, 21% (air) and a compressed gas cylinder of 40% in O_2 was used. The calibration curve used for measuring the concentration of O_2 in CO_2 was carried out using compressed bottles of CO_2 mixtures in N_2 at 2%, 10%, 20%, 40% and 50% CO_2.

The results of the oxygen concentration measured at the reactor inlet are shown in Fig. AIII.1, for both atmospheres (i.e. O_2/N_2 and O_2/CO_2), with O_2 concentrations from 11% to 80%. Four identical measurements were carried out for each case. On the one hand, the results show a dispersion in experimental measures for each concentration less than 1%. On the other hand, the measured O_2 concentration agree with the calculated results (differences less than 2%).

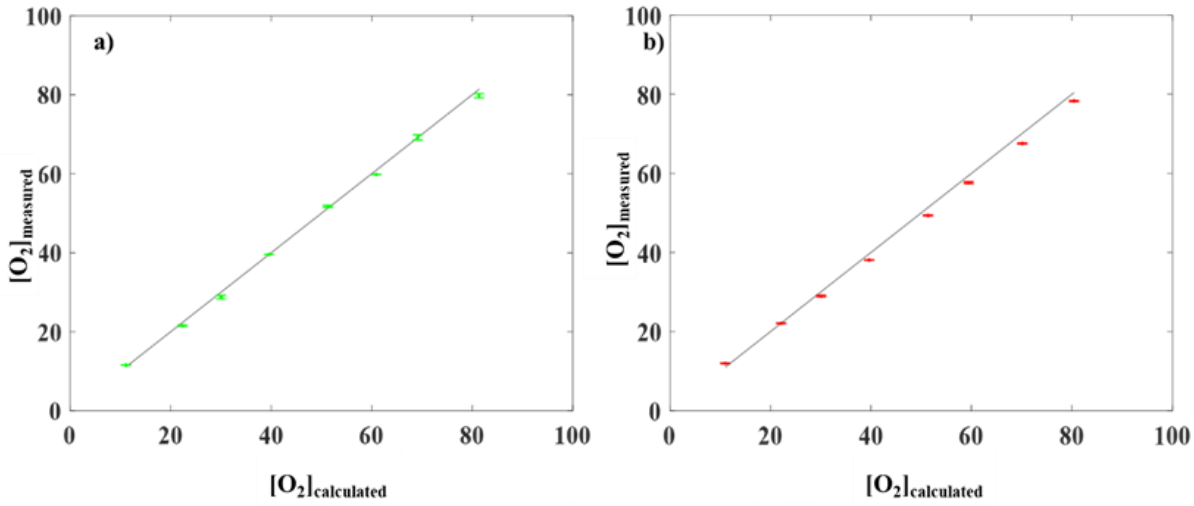

Figure AIII.0.1 O_2 concentration calculated vs measured at the reactor inlet in O_2/N_2 (a) and O_2/CO_2 (b) atmosphere.

Appendix IV
Effect of the filter on the radiation captured by the camera

The maximum temperature of the char particle that can be measure by calibration performed in previous work is 1020 ºC, which is reached for 40% O_2 concentrations in N_2 (Figure AIV.1). One of the tasks of this work is understand the effect of CO_2 at higher O_2 concentration. In order to solve this problem a neutral density filter was collocated on the digital camera. This filter has three positions. The change of position darkens the image gradually. The attenuation of the radiation captured by the camera is expected, in order to reach the saturation of the technique at higher temperature. With the purpose of understanding the effect of the filter in the combustion tests some experiments were carried out.

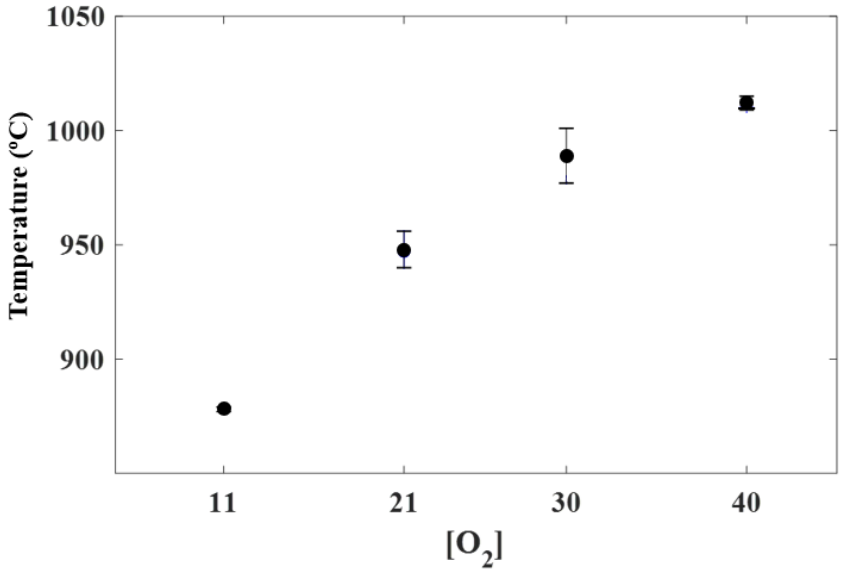

Figure AIV. 0.1 Results of maximum temperatures obtained in previous works using biomass char particles in combustion tests in O2/N2 atmosphere at different O2 concentration, from 11% to 40% [26] .

IV.1 Experimental methodology

The experimental set up is like used in calibration tests and it is shown in Figure AIV.2. The temperature inside the furnace is measured by two K-type thermocouples. On the one hand, one of them (1.5 mm sheath diameter) is used to control the temperature during the test, so it is connected to the oven by a PID controller. On the other hand, the second thermocouple is connected to a datalogger, and it allows to record the temperature during the test and save its history.

A thermal insulation material (rockwool) is positioned on the quartz window to cover part of the visible area. The probes of the two thermocouples installed inside the furnace are collocated in the free region (on the inner side of the window), and this section is, at the same time, the selected area for the subsequent analysis. In this way, the temperature measure by the thermocouples correspond with the brightness of the selected section (Figure AIV.3).

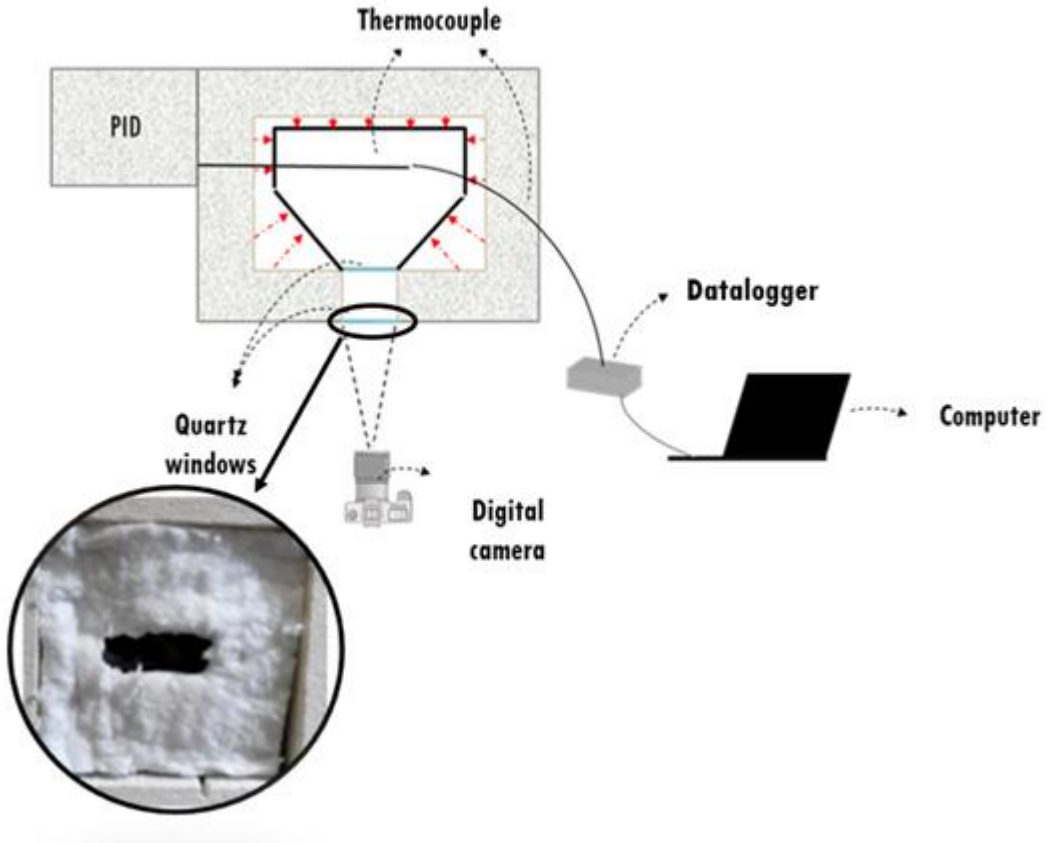

Figure AIV. 0.2 Experimental set up for the experiments to understand the effect of the filter.

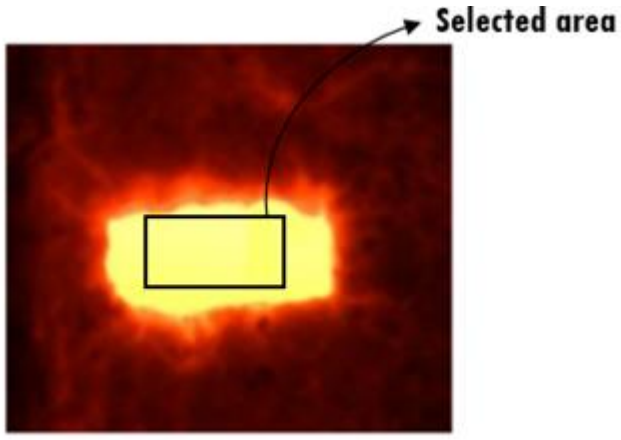

Figure AIV.0.3 Selected area used on the temperature analysis

The recording starts when the temperature inside the furnace reaches to 600ºC (at lower temperature the digital number values assigned by the digital camera are nulls). Then, the oven temperature is increased from 600ºC to 1100ºC (maximum temperature reached by the furnace). This procedure is applied to experiments using a filter in each position (cases B, C and D) and also, without using a filter (case A).

IV.1 Experimental results

When the frames are generated from the video using Adobe Premier CS6, the average of the digital number values, from each spectral band (red, green and blue), associated with the pixels of the selected area, are determined using Matlab.

The DN-T curves obtained are shown in Figure AIV.4. In the cases in which the filter is used (Case B, C and D), the digital numbers values assigned by the camera for the same temperature are below the values in the case A. An important aspect in this series of experiments is that the higher position of the filter, the lower digital number associated by the camera for the same temperature. In practice, this means that choosing higher position of the filter enables measuring higher temperature. The consequence of moving the filter to higher position is that the DN-T curves are displaced in the x-axis. All colors are displaced in the same quantity. The distance the magnitude of the displacement is the same for all DN-T curves, i.e. for the three spectral bands.

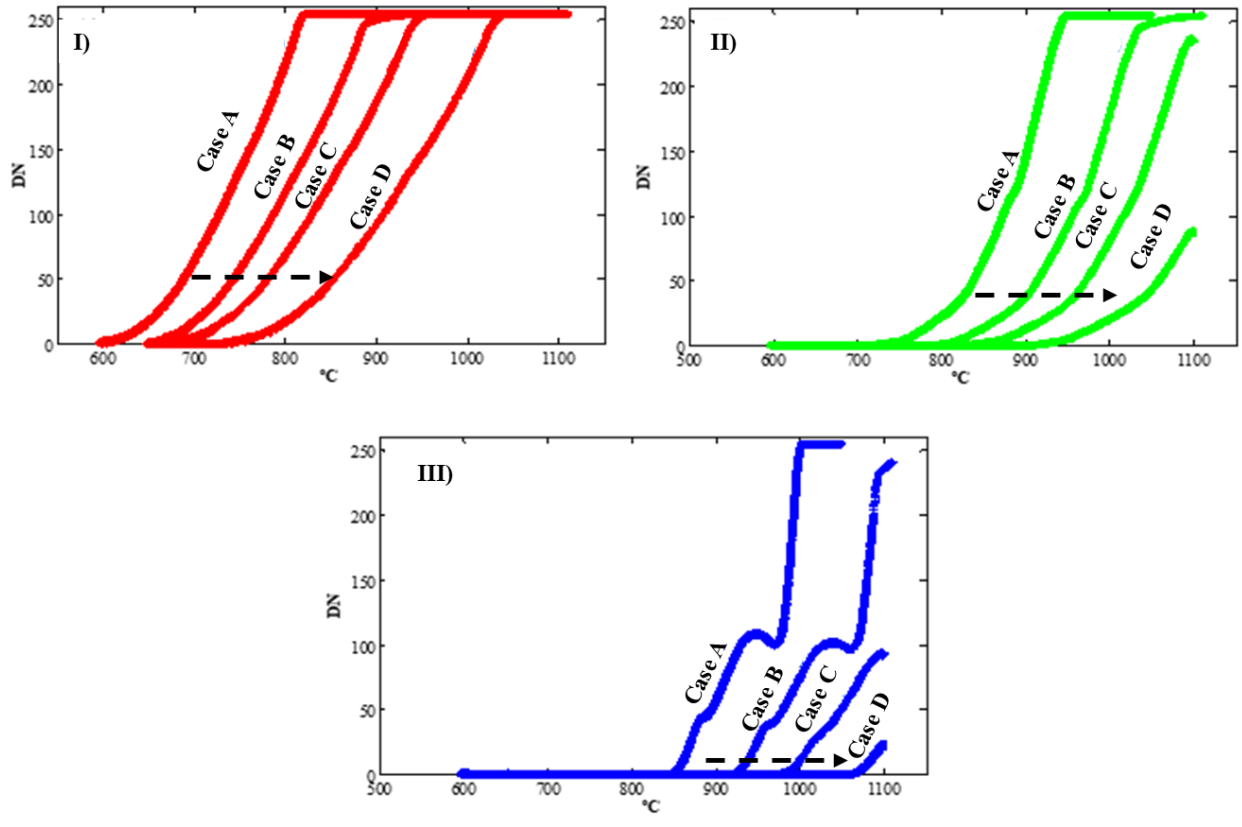

Figure AIV.0.4 Digital numbers red (I), green (II) and blue (III) assigned by the camera when the filter is not used (A) and when the filter has the position 1 (B), 2 (C) and 3 (D), versus the temperature measured with thermocouple.

In other to measure a high temperature as possible, the position number 3 of the filter (Case D) was chosen for the combustion tests.

It is noteworthy that the DN_b-T curve (Figure AIV.4 C) shows a change of trend. It is suspected that this unreasonable behavior is an artifact of the camera software. Therefore, to avoid misleading results the maximum temperature is taken from the part of the curve that is reliable.

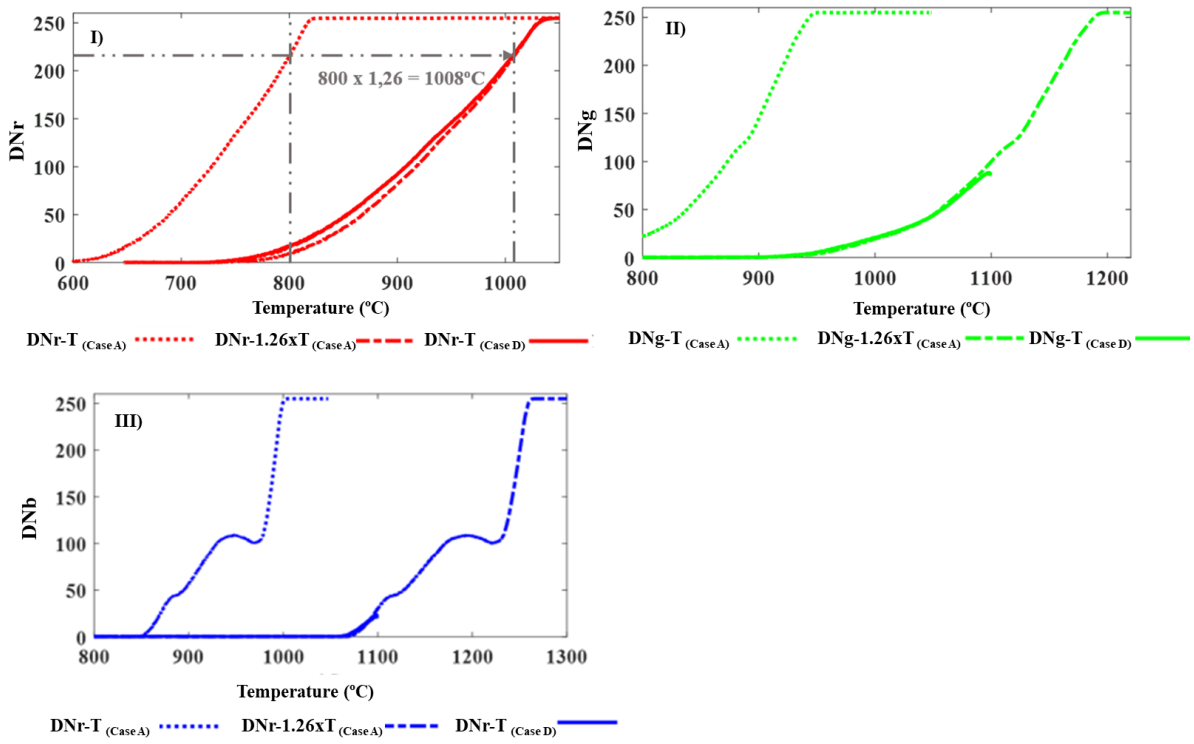

Figure AIV.0.5 DN-T curves for each spectral band (red(I), green(II) and blue(III)) in case A (without filter), case D (filter in the last position) and DNk-T curves calculated using the direct proportional relation between case A and D (eq. AIV.1).

Appendix V. Results and validation of the calibration methodology

1. Experimental results

The DN_k numbers are given by the digital camera and the temperatures are measured with a thermocouple as described above. The lower and higher energy levels of the sensor, which correspond to the minimum and maximum digital numbers (DN) of the pixels, determine the minimum and maximum temperatures measurable in each spectral band. For instance, in the color red band (k= color red), the DN ranges from 0 to 255, which translates to temperatures in the range of 650ºC to 1022 ºC. Above a DN of 255 the signal of the red band is saturated, and the temperature cannot be measured. The correlation between DN and measurable temperature for the three spectral bands are displayed in Figure AV.0.1.

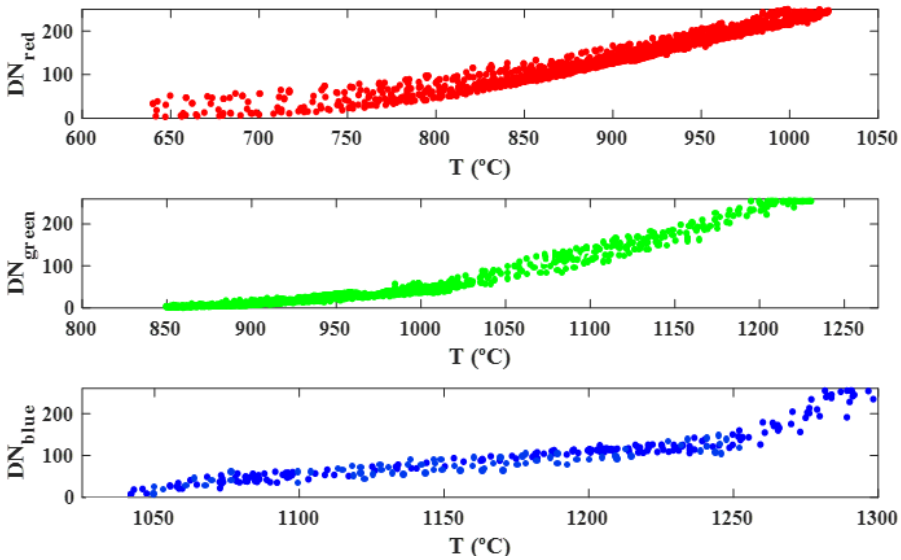

Figure AV.0.1 DN-T Red (a), green (b) and blue (c) digital numbers vs. measured temperature by the thermocouple inserted in the gap made on particle surface.

The lower numbers of points used to draw the calibration curve at temperatures higher than 1250 ºC is due to the practical difficulties to reach such high temperatures. For instance, the higher temperature range is reached at high conversion degree, when the particles are too small to hold the thermocouple. The dispersion of the data is discussed in the validation section below.

2. Calculation of the empirical parameter β_k

As it is explained above, with a pyrometry method using a digital camera, the parameter β_k is the objective in the calibration process. For each DNk-temperature par, there is a single β_k value, which is derived from the experimental DNk- temperature curves above (Figure AV.0.1.) and using (3.2) Grey-body behavior for the char particle (i.e. 0.85 emissivity [49,50]) has been assumed in (3.2). The $\ln(DN_k)$– $\ln(\beta_k)$ curves are shown

in Figure Figure AV.0.2 and they are fitted to a quadratic equation (3.3) with the coefficients listed in Table AV.01.

$$\ln(\beta_{P1C,k}) = \alpha_{P1C,k} \ln (DN_k)^2 + \gamma_{P1C,k} \ln(DN_k) + \delta_{P1C,k} \quad \text{(AV.1)}$$

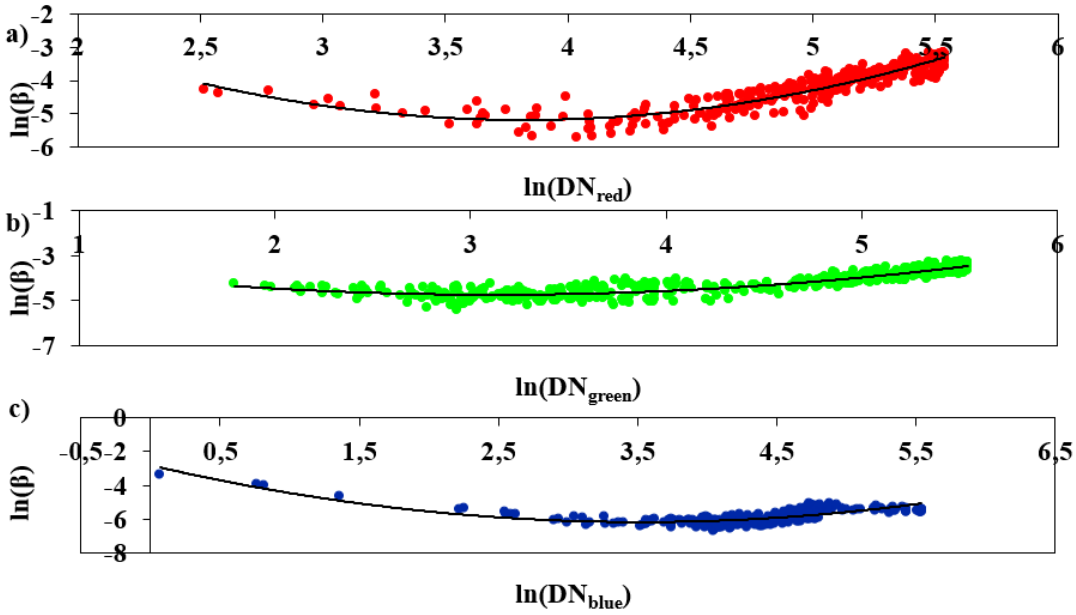

Figure AV.0.2 Red (a), green (b) and blue (c) digital numbers and. calibration parameter β relation, experimental results (color points) and fitting curves (black line)

Table AV.0.1 Fitting coefficients for the calibration curves.

	α	γ	δ	R^2
Red	0.6394	-4.8864	4.1494	0.8499
Green	0.2187	-1.3664	-2.6082	0.7945
Blue	0.2701	-1.9027	-2.8064	0.6119

2.3 Validation

The accuracy of the temperature measured by pyrometry has been assessed by the deviation from the temperature measured by the thermocouple (i.e. absolute error), which is displayed in Figure AV.02b and it is calculated according to (3.2). $T_{pyrometry}$ represents the temperature measured by pyrometry as given by the calibration method for the DN indicated by the digital camera; while $T_{thermocouple}$ refers to the temperature measured by the thermocouple for the same case. As described in above, there are several repeat measurements of $T_{thermocouple}$, i.e. a range of $T_{thermocouple}$, for each DN (or $T_{pyrometry}$). Therefore, the error has been

estimated for the range of T_{tp} values. The range of T_{tp} measurements for each T_{pyr} is shown in Figure 3.9 a.

$$e(°C) = \left\| T_{pyrometric} - T_{thermocouple} \right\| \quad (3.4)$$

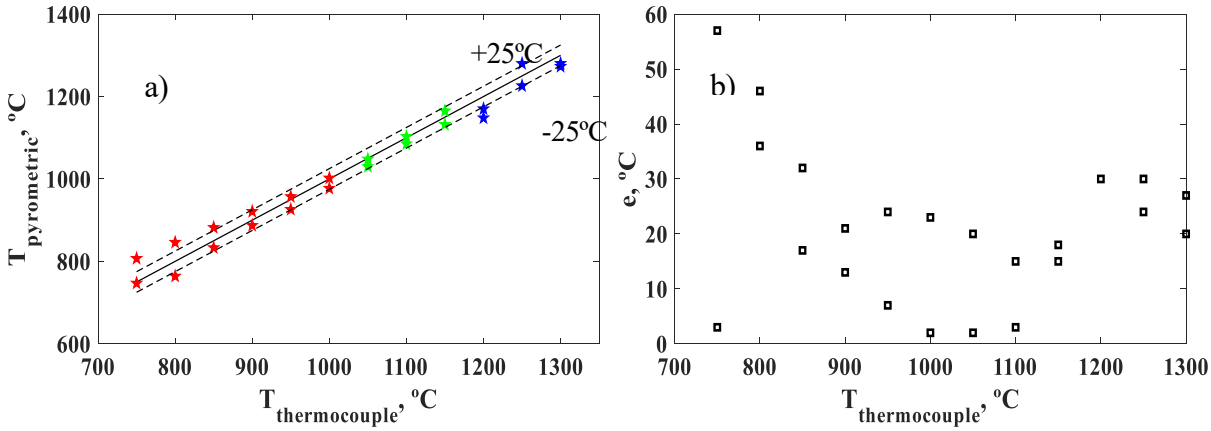

Figure AV0.1 Precision of the pyrometry method in the three spectral bands. (a) Range of temperatures measured by the thermocouple for each temperature indicated by the pyrometry method. (b) Absolute error according to (3.4) Each band is represented in its own color. $T_{thermocouple}$: temperature shown by the thermocouple. $T_{pyrometric}$: temperature measured by the pyrometry method.

Deviations from the temperature measured with the thermocouple larger than 50 ºC are not deemed accuracy enough for the purpose of this work. This threshold is based on a previous publication [26,49], which showed that the maximum particle temperature obtained at two consecutive O_2 concentrations (e.g. 11%-21%-30%) differed in approximately 50 ºC. Thus, accuracy of at least 50ºC is required to claim a difference in temperature between two measurements.

As shown in Fig. 3.9 b, the absolute error of the temperature measured by pyrometry is above the accuracy threshold in the temperature ranges T_{pyr}<850 ºC. For temperatures below 850 ºC, the lack of accuracy can be related to a time mismatch between the thermocouple datalogger and the digital camera recording. A time mismatch of milliseconds in this range of temperature can cause differences larger than 40ºC, as this range corresponds to the beginning of the conversion when the temperature of the particle increases rapidly. This range of temperature has, therefore, been excluded from the analysis.

The reproducibility of the calibration method is tested by comparing the results obtained in this work to those obtained in similar conversion tests and applying the same pyrometry method, where the calibration of the digital camera was carried out without filter [49,50]. Figure 3.10 shows the temperature measured by pyrometry over conversion time for tests conducted at 21% and 40% O_2 in N_2. T_{min} refers to the particle temperature in the emulsion phase, whereas T_{max} refers to the temperature of the particle in the splash zone and the bubble phase. Figure 3.11 shows the maximum temperatures of the particle as a function of the O_2 concentration (O_2/N_2), with the standard deviation of the measurements. The figure includes both measurements carried out in this work and those from Salinero et al. [26].

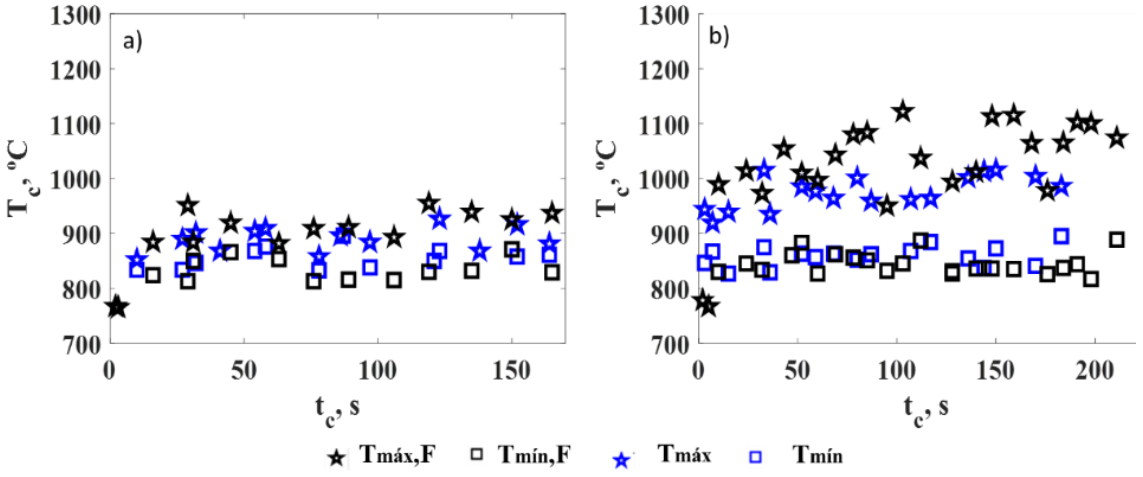

Figure 0.2 Minimum and maximum particle temperature measured by pyrometry over conversion time of a beech particle of 8mm diameter (a) 21% O_2/N_2; (b) 40% O_2/N_2. Blue symbols from Salinero et al. [26]. Black symbols from this work.

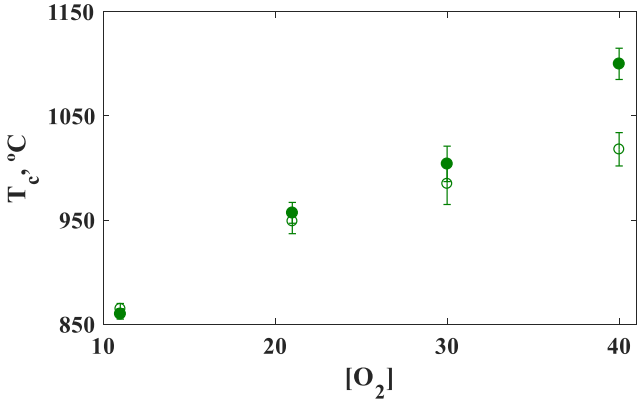

Figure 0.3 Maximum superficial temperature of the char particle versus O_2 in N_2. Filled symbols: results with filter from this work. Empty symbols: results without filter from Salinero et al. [26].

Up to 30% O_2, there is a good agreement of the temperature results derived from the two works. However, for higher O_2 concentrations the results obtained in the previous work are significantly lower than those obtained here, which can be explained by the saturation of the measurement method when the filter was not applied (i.e. [26, 49]). In their case, the method was not able to measure temperatures above 1020ºC (Figure 3.11).